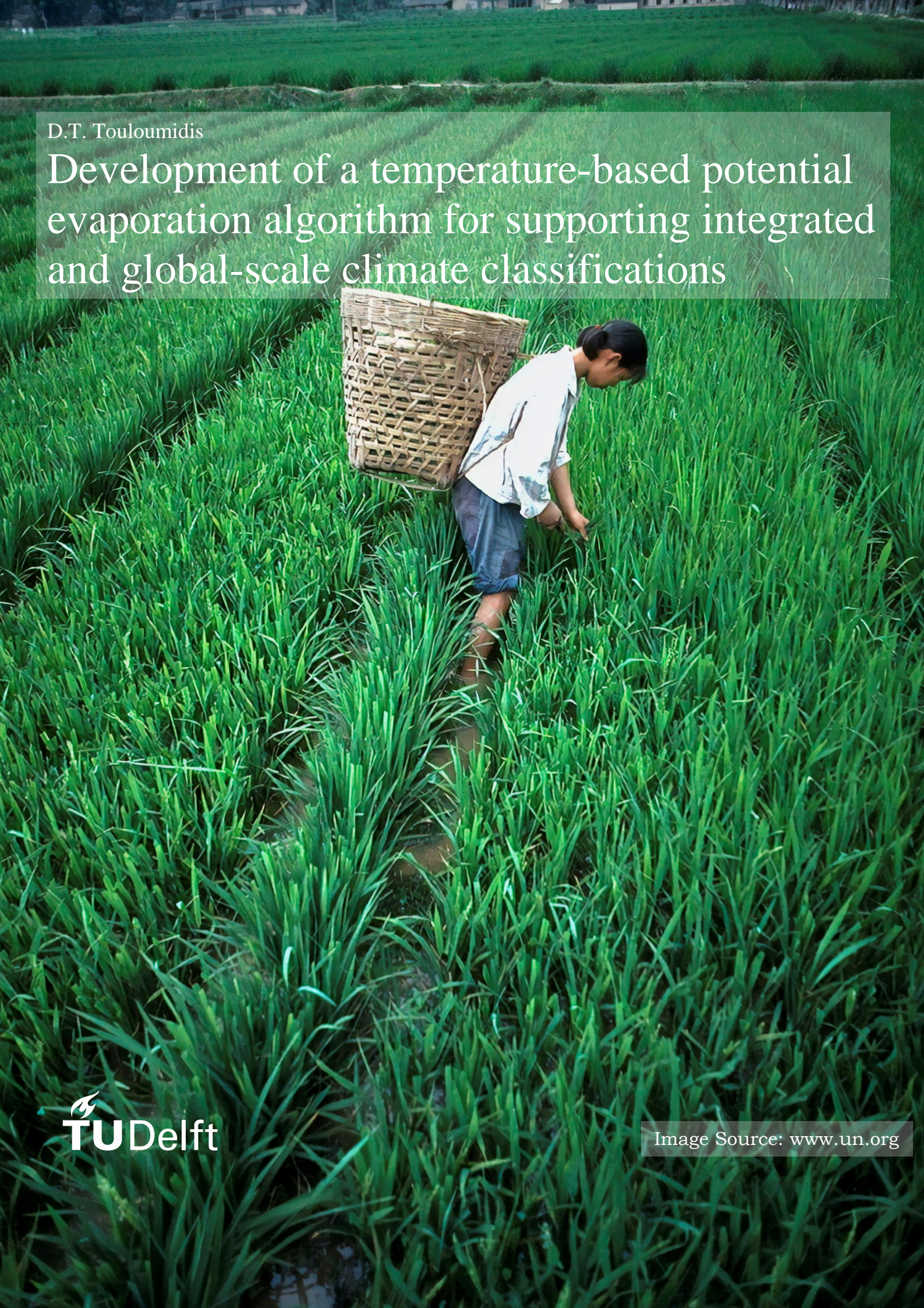


D.T. Touloumidis

Development of a temperature-based potential evaporation algorithm for supporting integrated and global-scale climate classifications



Development of a temperature-based potential evaporation algorithm for supporting integrated and global-scale climate classifications

By

D.T. Touloumidis

in partial fulfilment of the requirements for the degree of

Master of Water Management
in Civil Engineer

at the Delft University of Technology

Supervisors:

Dr ir. A.M.J. Coenders, TU Delft
Dr ir. Marie-Claire ten Veldhuis,
TU Delft

Advisor:

Dr V. Aschonitis, Greek Institute of Soil
and Water Resources



Contents

Abstract	1
Acknowledgements	2
1. Introduction	3
2. Materials and Methods	7
2.1. Method.....	7
2.1.1. Derivation/calibration of Thornthwaite correction factor for short reference crop based on ASCE-standardized method.....	7
2.1.2. Variation of Thornthwaite correction factor in major climate groups of Köppen-Geiger climate classification	9
2.1.3. Validation of C_{th} based on stations data	9
2.1.4. Evaluation of C_{th} use in aridity and aridity/humidity indices based on stations data	10
2.2. Data	11
3. Results	14
3.1. Derivation of the C_{th} correction factors and analysis of its variation in major Köppen-Geiger groups.....	14
3.2. Validation of the C_{th} correction factors.....	16
3.3. Evaluating the use of C_{th} factor in aridity indices	19
4. Discussion	22
4.1. The validity of the derived C_{th} of 1950-2000 for periods after 2000.....	22
4.2. Scale effects on the accuracy of the derived C_{th}	23
4.3. Justifications about the methodology for deriving annual C_{th} correction factors based on partial weighted averages.....	24
5. Conclusions	26
Bibliography	27
Supplementary Material	32

Table of Figures

Figure 2.1:	(a) 60 stations of California from CIMIS database, (b) 80 stations of Australia from AGBM database, and (c) 385 stations of Europe from ECAD database.....	12
Figure 2.2:	(a) Mean annual temperature between 1950 and 2000 (Hijmans et al., 2005), (b) Mean annual precipitation for the period of 1950-2000 (Hijmans et al., 2005), (c) mean annual reference evaporation of ASCE-standardized method for short reference crop between 1950 and 2000 (Aschonitis et al., 2017).	13
Figure 3.1:	(a) Global map of the annual partial weighted average C_{th} factors, (b) Köppen-Geiger climate classification map, (c) sampling points distribution.	15
Figure 3.2:	HPD distributions of C_{th} per each major Köppen-Geiger group and f) for all Köppen-Geiger groups (excluding places where $C_{th}=0$)	15
Figure 3.3:	<i>Left side:</i> 1:1 plots of mean monthly E_p (Eq.1) versus mean monthly E_r (Eq.4) (a) for 60 CIMIS stations of California, (c) for 80 AGBM stations of Australia and (e) for 385 ECAD stations of Europe, and <i>Right side:</i> 1:1 plots of mean monthly E_{ps} (Eq.11) versus mean monthly E_r (Eq.4) (b) for 60 CIMIS stations of California, (d) for 80 AGBM stations of Australia and (f) for 385 ECAD stations of Europe.	17
Figure 3.4:	<i>Left side:</i> 1:1 plots of mean annual E_p (Eq.1) versus mean annual E_r (Eq.4) (a) for 60 CIMIS stations of California, (c) for 80 AGBM stations	

	of Australia and (e) for 385 ECAD stations of Europe, and <i>Right side:</i> 1:1 plots of mean annual E_{ps} (Eq.11) versus mean annual E_r (Eq.4) (b) for 60 CIMIS stations of California, (d) for 80 AGBM stations of Australia and (f) for 385 ECAD stations of Europe. 18
Figure 3.5:	1:1 plots of (a) mean monthly E_p (Eq.1) versus mean monthly E_r (Eq.4), (b) mean monthly E_{ps} (Eq.11) versus mean monthly E_r (Eq.4), (c) mean annual E_p (Eq.1) versus annual monthly E_r (Eq.4), (d) mean annual E_{ps} (Eq.11) versus annual monthly E_r (Eq.4), using the data of all 525 stations from the three databases of CIMIS, AGBM, ECAD. . 19
Figure 3.6:	1:1 log-log plots of (a) A_{IUNEP} using mean monthly E_p (Eq.1) versus A_{IUNEP} using mean monthly E_r (Eq.4), (b) A_{IUNEP} using mean monthly E_{ps} (Eq.11) versus mean monthly E_r (Eq.4) using the data of all 525 stations from the three databases of CIMIS, AGBM, ECAD..... 20
Figure 3.7:	1:1 log-log plots of (a) A_{ITH} using mean monthly E_p (Eq.1) versus A_{ITH} using mean monthly E_r (Eq.4), (b) A_{ITH} using mean monthly E_{ps} (Eq.11) versus mean monthly A_{ITH} (Eq.4) using the data of all 525 stations from the three databases of CIMIS, AGBM, ECAD. 21
Figure 4.1:	1:1 plots of (a) mean monthly E_r of grids 1950-2000 (Fig.2.2c) vs. E_r of 525 stations raw data and (b) C_{th} of grids 1950-2000 (Fig.3.1a) vs. C_{th} of 525 stations estimated by their raw data. The values of grids correspond to the same positions of stations. 23
Figure 4.2:	1:1 plots of (a) of mean monthly E_{ps} (Eq.11) versus mean monthly E_r (Eq.4) and (b) of mean annual E_{ps} (Eq.11) versus mean annual E_r (Eq.4) for 60 CIMIS stations of California using the average value of their C_{th} values (i.e., equal to 1.66 for all stations) for the period 1950-2000..... 24
Figure 4.3:	Monthly values of original Thornthwaite $E_{p,i}$ and ASCE $E_{r,i}$ method together with their respective monthly correction factors for a position close to Garda Lake in Italy (10.124° E, 45.45° N). 25
Figure 4.4:	Simple linear regression analysis without intercept between monthly values of original Thornthwaite $E_{p,i}$ and ASCE $E_{r,i}$ from Figure 4.3.... 25

Table of Tables

Table 1.1:	Different models for the calculation of the reference evaporation. 3
Table 2.1:	Description of Köppen-Geiger climate classification symbols and defining criteria. Error! Bookmark not defined.
Table 2.2:	Description and characteristics of statistical criteria 10
Table 3.1:	General statistics and 2.5% and 97.5% thresholds of HPDs given in Fig.4 for the C_{th} values of each major Köppen-Geiger group and all groups..... 15
Table 3.2:	Statistical metrics (Eqs.12-16) for the comparisons between E_p vs. E_r and E_{ps} vs. E_r for CIMIS-California, AGBM-Australia and ECAD-Europe stations for (a) mean monthly and (b) mean annual analysis..... 18
Table 3.3:	Statistical metrics (Eqs.12-16) for the evaluation between E_p vs. E_r and E_{ps} vs. E_r when they are applied in the (a) A_{IUNEP} and (b) A_{ITH} aridity indices considering only non-humid or humid classes based on the data of all 525 stations from the three databases of CIMIS, AGBM, ECAD. 21

Abstract

The assessment of potential evaporation or reference combined evaporation and transpiration is among the most important components for many hydro-climatic projects, for example, irrigational networks' design and management, water-cycle balance assessment studies, and assessment of aridity classification indices. Aridity classification indices such as UNEP, Thornthwaite and others are usually employed at large scale applications and require respective estimations of potential or reference combined evaporation and transpiration. The major problem in such applications is not only the limited availability of stations per se but also the limitation of many stations to provide data for a complete set of parameters such as rainfall (P), temperature (T), solar radiation (R_s), wind speed (u) and relative humidity (H_R). A complete set of climate parameters is prerequisite for accurate estimations of potential or reference combined evaporation and transpiration using the most advanced methods, which are expressions of energy balance (e.g., ASCE-standardized method, successor method of Penman-Monteith FAO-56). Unfortunately, large scale applications of aridity indices suffer from this limitation and the common solution is to use temperature-based formulas. The most popular and historical temperature-based formula is the one of Thornthwaite, which was developed to support the respective aridity classification index. The popularity of this formula is highly connected to a minimum requirement of average temperature per month and latitude at the location of interest. Considering the above, this study aims to develop a global database of local correction factors for the original Thornthwaite formula that will better support all hydro-climatic applications but mostly to support large scale applications of aridity indices, which are highly prone to data limitations. The hypothesis that is tested in this work is that a local correction factor that integrates the local mean effect of aforementioned climate parameters (R_s , H_R , u) can improve the performance of the original Thornthwaite formula and to convert it at the same time to a formula of reference combined evaporation and transpiration for short reference crop. The global database of local correction factors was developed using gridded climate data of the period 1950-2000 with grid size ~ 1 km at the equator which corresponds to 30 arc-sec spatial resolution from freely available climate geodatabases. The correction factors were produced as partial weighted averages of monthly ratios between the benchmark ASCE-standardized method for short reference crop versus the original formula of Thornthwaite by giving more weight to the warmer months and by excluding colder months of $E_{pr} < 45$ mm month⁻¹ where monthly ratios are highly unstable with unrealistic values. The validation of the correction factors was made using raw data from 525 stations of Europe, California-USA and Australia that cover periods mostly after 2000 and up to 2020. The validation procedure showed significant improvement in the estimations of reference combined evaporation and transpiration using the corrected Thornthwaite formula that led to a 19.4% reduction of RMSE for monthly and a 55% reduction of RMSE for annual estimations compared to the original formula. The variation of the correction factor was also investigated in different major Köppen climate classes and it was found that tends to increase in drier and warmer territories. The five major Köppen groups were ordered as follows $B > C > A > D > E$ considering the magnitude of the correction factors values. The corrected and original Thornthwaite formulas were also evaluated by their use in UNEP and Thornthwaite aridity indices using as a benchmark the respective indices estimated by the ASCE-standardized method. The analysis was made using the validation data of the stations and the results showed that the corrected Thornthwaite formula increased by 18.3% the accuracy of detecting identical aridity classes with ASCE-standardized method for the case of UNEP classification, and by 10.4% for the case of Thornthwaite classification in comparison to the original formula. The performance of the corrected formula was extremely improved especially in the case of non-humid classes of both aridity indices. The overall results revealed that the correction factors derived in this study can improve the performance of the original Thornthwaite formula providing better estimations of the aridity classification indices.

Acknowledgements

For the accomplishment of my additional thesis, I would like to thank my supervisors Dr ir. Coenders and Dr ir. ten Veldhuis and my advisor Dr Aschonitis who made it possible and supported my work through their valuable guidance. My research was upgraded and my thinking was actively triggered by your suggestions and your advice.

Introduction

The current discussion about climate change focuses often on how much the temperature will rise over the coming century. However, climate change cannot be described only by temperature since also precipitation and other climate parameters (e.g., humidity, radiation, wind speed) all together affect the climate. Additionally, their changes should not be analyzed separately, because together they affect the evaporation, and many theoretical climatic fields (e.g., climate classification methods, aridity indices etc.) in order to detect any possible changes. One of the basic problems in climate analysis methods is that they are based on evaporation, which is a complex process that is regulated by many factors such as temperature, relative humidity, solar radiation and wind speed. In most cases, climate databases or individual stations cannot provide a complete set of these parameters but what they can provide is at least temperature and precipitation. Evaporation is a process where the liquid water is changing state, using specific energy and becomes water vapour (vaporization). Three types of evaporation will be discussed to determine the differences: actual, potential and reference evaporation. The actual evaporation is the summary of all direct evaporation processes (open water evaporation, soil evaporation, interception evaporation and snow or ice evaporation), it is an important term of the water balance equation and is constrained by the water availability. Actual evaporation is difficult to be measured, so instead, the potential evaporation is calculated, because it can be calculated without the constrain of water availability. The relationship between actual and potential evaporation is that the actual is a proportion of the potential and the potential is setting the upper limit of the possible evaporation (Luxemburg & Coenders A., 2017). For the first time, the term combined evaporation and transpiration was introduced in the early 80s to incorporate the properties of an ideal grass crop in specific conditions and it is calculated using the potential evaporation multiplied with the crop factor of each specific crop (Brouwer & Heibloem, 1986; Irmak, 2008). Hereinafter, the reference combined evaporation and transpiration will be referred to as reference evaporation (E_r), for the sake of convenience. Many research studies have been done to derive empirical equations for the reference evaporation with reduced climate parameters; some of them are considered temperature-based, some of them are radiation-based and others are mass-transfer based.

Table 1.1: Different models for the calculation of the reference evaporation.

Model	Formula	Climate data
Alexandris et al. (2006)	$E_r = 0.057 + 0.227 \cdot C_2 + 0.634 \cdot C_1 + 0.0124 \cdot C_1 \cdot C_2$ <p>where: $C_1 = 0.6416 - 0.00784 \cdot H_R + 0.372 \cdot R_S - 0.00264 \cdot R_S \cdot H_R$ $C_2 = -0.0033 + 0.00812 \cdot T_{mean} + 0.101 \cdot R_S + 0.00584 \cdot R_S \cdot T_{mean}$</p>	T_{mean}, R_S, H_R
Baier and Robertson (1965)	$E_r = 0.09 \cdot (1.67021 \cdot T_{max} + 1.68085 \cdot TD + (1.159575 \cdot R_a) - 57.3404)$	T_{max}, T_{min}

	$E_r = 16 \cdot \left(10 \cdot \frac{0.36 \cdot (3 \cdot TD)}{J} \right)^a \cdot \frac{N \cdot n}{365}$	
Camargo et al. (1999)	$J = \sum_{i=1}^{12} j_i$	T_{max}, T_{min}
	$j_i = \left(\frac{T_{mean, i}}{5} \right)^{1.514}$	
	$\alpha = (6.75 \cdot 10^{-7}) \cdot J^3 - (7.71 \cdot 10^{-5}) \cdot J^2 + (1.79 \cdot 10^{-2}) \cdot J + 0.492$	
Droogers and Allen (2002)	$E_r = 0.00102 \cdot (T_{mean} + 16.8) \cdot R_a \cdot (TD)^{0.5}$	$T_{mean}, T_{max}, T_{min}$
Droogers and Allen (2002)	$E_r = 0.000530 \cdot (T_{mean} + 17.0) \cdot (TD - 0.0123 \cdot P)^{0.76}$	$T_{mean}, T_{max}, T_{min}, P$
Hargreaves and Samani (1982, 1985)	$E_r = c \cdot 0.408 \cdot (T_{mean} + 17.8) \cdot R_a \cdot (TD)^{0.5}$	$T_{mean}, T_{max}, T_{min}$
Aschonitis et al. (2017)	where: $c = 0.0023$ (original value) $c = c_{HS}$ (local coefficient from global grid)	
Hammon (1961)	$E_r = 13.97 \cdot \left(\frac{n}{12} \right)^2 \cdot \frac{e^o(T_{mean})}{1000}$	T_{mean}
Hammon (1963)	$E_r = 0.1651 \cdot \frac{n}{12} \cdot \frac{21.67 \cdot e^o(T_{mean})}{T_{mean} + 273.3}$	T_{mean}
Makkink (1957)	$E_r = 0.61 \cdot \frac{\Delta}{\Delta + \gamma} \cdot \frac{R_s}{\lambda} - 0.12$	T_{mean}, R_s
Malmström (1969)	$E_r = 0.409 \cdot e^o(T_{mean})$	T_{mean}
McCloud (1955)	$E_r = 0.254 \cdot 1.07^{1.8 \cdot T_{mean}}$	T_{mean}
Papadakis (1962)	$E_r = 0.5625 \cdot (e^o(T_{max}) - e^o(T_{min} - 2))$	T_{min}, T_{max}
Allen et al. (2005)	$E_r = \frac{0.408 \cdot \Delta \cdot (R_n - G) + \frac{\gamma \cdot u_2 \cdot (e_s - e_a) \cdot C_n}{(T_{mean} + 273.16)}}{\Delta + \gamma \cdot (1 + C_d \cdot u_2)}$	T_{mean}, R_s, H_R, u_2
Priestley and Taylor (1972), Aschonitis et al. (2017)	$E_r = a \cdot \frac{0.408 \cdot \Delta}{\Delta + \gamma} \cdot (R_n - G)$ where: $a = 1.36$ (original value) $a = \alpha_{PT}$ (local coefficient from global grid)	$T_{mean}, T_{max}, T_{min}, R_s$
Oudin et al. (2005)	$E_r = 0.408 \cdot R_a \cdot 0.01 \cdot (T_{mean} + 5) \text{ if } T_{mean} > 5^\circ\text{C}$ $E_r = 0 \text{ if } T_{mean} \leq 5^\circ\text{C}$	T_{mean}
Oudin et al. (2005)	$E_r = \left(\frac{n}{12} \right)^2 \cdot \exp\left(\frac{T_{mean}}{16} \right)$	T_{mean}
Thorntwaite (1948)	$E_p = 16 \cdot \left(\frac{10 \cdot T_{mean}}{J} \right)^a \cdot \frac{N \cdot n}{365}$ $J = \sum_{i=1}^{12} j_i,$ $j_i = \left(\frac{T_{mean, i}}{5} \right)^{1.514}$ $\alpha = (6.75 \cdot 10^{-7}) \cdot J^3 - (7.71 \cdot 10^{-5}) \cdot J^2 + (1.79 \cdot 10^{-2}) \cdot J + 0.492$	T_{mean}
Turc (1961)	$E_r = 0.013 \cdot \left(\frac{T_{mean}}{T_{mean} + 15} \right) \cdot \frac{23.88 \cdot R_s + 50}{\lambda} \text{ for } H_R \geq 50\%$ $E_r = \left(1 + \frac{50 - H_R}{70} \right) \cdot 0.013 \cdot \left(\frac{T_{mean}}{T_{mean} + 15} \right) \cdot \frac{23.88 \cdot R_s + 50}{\lambda} \text{ for } H_R < 50\%$	T_{mean}, R_s, H_R
WMO (1966)	$E_r = 0.1 \cdot (1.298 + 0.00934 \cdot u_2) \cdot (e_s - e_a)$	$T_{min}, T_{max}, H_R, u_2$
Valiantzas (2013, 2014)	$E_r = 0.0393 \cdot R_s \cdot \sqrt{T_{mean} + 9.5} - 0.19 \cdot R_s^{0.6} \cdot \varphi^{0.15} + 0.0061 \cdot (T_{mean} + 20) \cdot (1.12 \cdot T_{mean} - T_{min} - 2)^{0.7}$	T_{mean}, T_{min}, R_s

$$E_r = 0.0393 \cdot R_s \cdot \sqrt{T_{mean} + 9.5} - 0.19 \cdot R_s^{0.6} \cdot \varphi^{0.15} + 0.078 \cdot (T_{mean} + 20) \cdot \left(1 - \frac{H_R}{100}\right) \quad T_{mean}, R_s, H_R$$

$$E_r = 0.0393 \cdot R_s \cdot \sqrt{T_{mean} + 9.5} - 2.4 \cdot \left(\frac{R_s}{R_a}\right)^2 + Cu \cdot (T_{mean} + 20) \cdot \left(1 - \frac{H_R}{100}\right) \quad T_{mean}, R_s, H_R$$

where: $Cu = 0.054$ for $H_R > 65\%$ and $Cu = 0.083$ for $H_R \leq 65\%$

E_r : is the reference crop evaporation (mm d^{-1}), T_{mean} , T_{max} , T_{min} : Mean, maximum and minimum temperature ($^{\circ}\text{C}$), TD : difference between maximum and minimum temperature ($^{\circ}\text{C}$), R_s : incident solar radiation ($\text{MJ m}^{-2} \text{d}^{-1}$), R_n : the net radiation at the crop surface ($\text{MJ m}^{-2} \text{d}^{-1}$), u_2 : the wind speed at 2 m height above the soil surface (m s^{-1}), R_a : extraterrestrial solar radiation ($\text{MJ m}^{-2} \text{d}^{-1}$), H_R : relative humidity (%), Δ : slope of the saturation vapor pressure-temperature curve ($\text{kPa } ^{\circ}\text{C}^{-1}$), γ : psychrometric constant ($\text{kPa } ^{\circ}\text{C}^{-1}$), G : the soil heat flux density at the soil surface ($\text{MJ m}^{-2} \text{d}^{-1}$), e_s : the saturation vapor pressure (kPa), e_a : the actual vapor pressure (kPa), $e^{\circ}(T)$: saturation vapor pressure at air temperature T (kPa), φ : absolute value of latitude (rads), P : precipitation (mm month^{-1}), n : number of days in the month, N : mean length of daylight of the days of the month (hours), J : annual heat index, j_i : monthly heat index, α : the function of the annual heat index, λ is the latent heat of vaporization in MJ kg^{-1} ($\lambda = 2.45 \text{ MJ kg}^{-1}$ at a temperature of 20°C). C_n and C_d : are constants, which vary according to the time step and the reference crop type and describe the bulk surface resistance and aerodynamic roughness. Eq.4 can be applied for two types of reference crop, this study focuses on the short reference crop (ASCE-short), which corresponds to clipped grass of 12 cm height and surface resistance of 70 s m^{-1} where the constants C_n and C_d have the values 900 and 0.34, respectively (Allen et al., 2005).

For the estimation of evaporation, there are many empirical equations (Table 1.1). The selection of the appropriate method, considering also climate data availability, has received considerable attention and has triggered remarkable debate (Trenberth, et al., 2014; Tegos, Malamos, & Koutsoyiannis, 2015; Rezaei, Valipour, & Valipour, 2016; Zhang, et al., 2016; Valipour, Gholami Sefidkouhi, & Raeini-Sarjaz, 2017; Feng, Trnka, Hayes, & Zhang, 2017). One of the most widely used potential evaporation models that were developed in the previous century is Thornthwaite's formula (Thornthwaite, 1948). This specific model requires only mean monthly temperature data and is a viable solution for a climatologist/hydrologist in case of reduced data. Estimations of global trends under climate change cause an argument due to the differences between the Penman-Monteith concept and Thornthwaite concept of reference evaporation assessments (Sheffield, Wood, & Roderick, 2012; Van Der Schrier, Barichivich, Briffa, & Jones, 2013; Trenberth, et al., 2014; Yuan & Quiring, 2014).

The Thornthwaite method is a simple and empirical scheme for calculating potential evaporation using only air temperature data and the maximum amount of sunshine duration as of function of latitude. In the Thornthwaite formula (Thornthwaite, 1948) the monthly mean temperature was correlated with evaporation using an exponential relationship, as determined from the water balance, for valleys in the central and eastern USA, where there was a supply of surface water. A modification of Thornthwaite's original approach was also presented by Willmott et al. (1985) by introducing a parameterization for a range of monthly mean temperature varying below zero and above 26.5 degrees Celsius. The Thornthwaite method overestimates the evaporation in humid climates and underestimates it in arid climates (Pereira & Pruitt, 2004; Castañeda & Rao, 2005; Trajkovic & Kolakovic, Evaluation of reference evapotranspiration equations under humid conditions, 2009a), and thus, many efforts have been made to amend the parameters or constants of the empirical formula to adapt it to various geographical zones (Jain & Sinai, 1985; Pereira & Pruitt, 2004; Castañeda & Rao, 2005; Zhang, Liu, Wei, Liu, & Zhang, 2008; Bakundukize, van Camp, & Walraevens, 2011; Yang, Ma, Zheng, & Duan, 2017). Jain and Sinai (1985) modified the constant in the general equation of

the Thornthwaite formula based on the min-max range of the annual mean air temperature in order to calculate the evaporation for semi-arid conditions. [Pereira and Pruitt \(2004\)](#) proposed an adaptation of the Thornthwaite scheme to estimate the daily evaporation in two contrasting environments in the USA and Brazil. [Castaneda and Rao \(2005\)](#) recalibrated the coefficient of the main equation of the Thornthwaite method based on estimations of reference evaporation using the FAO Penman-Monteith method in southern California. [Zhang et al. \(2008\)](#) used a modified formula to estimate the actual evaporation in cropland, shrubland and forest located in the subalpine region of southwestern China. [Bakundukize et al. \(2011\)](#) used two modifications and the original Thornthwaite method to groundwater recharge estimations in the inter-lacustrine zone of East Africa. [Yang et al. \(2017\)](#) presented a method to quantitatively identify the differences in the spatiotemporal variabilities of global drylands between the Thornthwaite and Penman-Monteith parameterizations for E_r .

The climate of an area is playing a key role in the aforementioned spatiotemporal variabilities. The first try to classify the climate of a specific area has been done by Köppen at the early of the 20th century and the middle of the same century, Geiger updated that classification. The aforementioned classification uses precipitation and temperature and contains 30 classes (3 tropical classes (A), 4 arid (B), 9 temperate (C), 12 cold (D) and 2 polar (E)); each class is coded with a three-digit system, the first element is representing the groups of vegetation, the second is representing the rainfall of the area and the last one (where is present), stands for the air temperature ([Kottek, Grieser, Beck, Rudolf, & Rubel, World map of the Köppen-Geiger climate classification updated, 2006](#)).

The climate change in terms of global warming is having an important impact on arid areas ([Kimura, 2020](#)) which are covering about the 40% of the continental Earth ([Ashraf, Yazdani, Mousavi-Baygi, & Bannayan, 2014](#)). The increasing carbon dioxide emissions are going to cause an increment of temperature that will result in water scarcity and drought in arid areas ([Kimura, 2020](#)). The role of aridity indices is very important to apply an integrated climate analysis of a region; many popular climate/aridity indices such as those of [UNEP \(1997\)](#), [Thornthwaite \(1948\)](#), [Holdridge \(1967\)](#) etc are based on formulas that require data of precipitation (P) and evaporation (E). In large scale applications of climate/aridity indices at country/continent/global scale, there is always the problem of data limitation for estimating evaporation E using methods that require complete data of climate parameters (i.e., temperature, solar radiation, relative humidity, wind speed). A solution to this problem is the use of temperature-based formulas of E ([Alexandris, Kerkides, & Liakatas, 2006](#); [Baier & Robertson, 1965](#); [Camargo et al., 1999](#); [Droogers & Allen, 2002](#); [Hargreaves & Samani, 1982](#); [Aschonitis, et al., 2017a,b](#); [Hamon W. R., 1963](#); [Hamon W. R., 1963](#); [Makkink, 1957](#); [Malmström, 2007](#); [Turc, 1961](#), [WMO, 1966](#); [Thornthwaite, 1948](#); [Allen et al. 2002](#)).

To sum up, the necessity of evaporation calculation lays to the fact that is a key variable of the water-cycle; the ASCE standardized Penman-Monteith method, which estimates the reference evaporation accurately, is taking four inputs, some of them are not easily measured (R_s , u , H_R). On the other hand, Thornthwaite's empirical formula is only using the average temperature and the latitude value for the calculation of the potential evaporation; accurate measurements of temperature are easy to be done or obtained from open source databases for the whole of the world. Considering the above, this study aims to develop a global database of local correction factors for the original Thornthwaite formula that will better support all hydro-climatic applications (irrigation design and management, water balance assessment studies, and even climate change assessment ([Muhammad et al. 2019](#); [Trajkovic 2007](#)) but mostly to support large scale applications of aridity indices, which are highly prone to data limitations. The hypothesis that is tested in this work is that a local correction factor that integrates the local mean effect of wind speed, humidity and solar radiation can improve the performance of the original Thornthwaite formula and to convert it at the same time to a formula of reference evaporation for short reference crop.

2

Materials and Methods

2.1. Method

2.1.1. Derivation/calibration of Thornthwaite correction factor

As it has been mentioned before, the calculation of reference evaporation with Penman-Monteith is often difficult due to lack of data that is needed; on the other hand, the empirical Thornthwaite formula is used for the calculation of the potential evaporation only using temperature and latitude. The original Thornthwaite model was calibrated with stations located in the east-central United States in humid climate conditions (Thornthwaite, 1948); though, many studies have shown that its application can be extended globally, over mid-latitude climate (Sepaskhah & Razzaghi, 2009). The following methodology will be applied to express the Penman-Monteith reference evaporation as a function of the Thornthwaite using a correction factor. The monthly potential evaporation using the Thornthwaite (1948) method is estimated as follows:

$$E_p = 16 \cdot \left(\frac{10 \cdot T_{mean}}{J} \right)^{\alpha} \cdot \frac{N \cdot n}{365} \quad (1)$$

$$J = \sum_{i=1}^{12} j_i,$$

$$j_i = \left(\frac{T_{mean,i}}{5} \right)^{1.514} \quad (2a,b,c)$$

$$\alpha = (6.75 \cdot 10^{-7}) \cdot J^3 - (7.71 \cdot 10^{-5}) \cdot J^2 + (1.79 \cdot 10^{-2}) \cdot J + 0.492$$

$$N = \frac{24}{\pi} \cdot \omega_s$$

$$\omega_s = \frac{\pi}{2} - \arctan \left[\frac{-\tan(\varphi) \cdot \tan(\delta)}{X^{0.5}} \right] \quad (3a,b,c)$$

$$\text{where: if } X \leq 0: X = 0.00001 \text{ else } X = 1 - [\tan(\varphi)]^2 \cdot [\tan(\delta)]^2$$

$$\delta = 0.409 \cdot \sin \left(2 \cdot \pi \cdot \frac{d_j}{365} - 1.39 \right)$$

where E_p : mean monthly potential evaporation of month i (mm month⁻¹), $T_{mean,i}$: mean monthly temperature (°C), n : number of days in the month, N : mean length of daylight of the days of the month (hours), J : annual heat index, j_i : monthly heat index, α : expression of annual heat index and d_j : Julian day.

The benchmark method that was used for developing correction factors for the temperature-based method of Thornthwaite is ASCE standardized method (former FAO-56), which estimates reference evaporation from short clipped grass, and it is estimated using the ASCE standardized method as it was proposed by Allen (2005):

$$E_r = \frac{0.408 \cdot \Delta \cdot (R_n - G) + \frac{\gamma \cdot u_2 \cdot (e_s - e_a) \cdot C_n}{(T_{\text{mean}} + 273.16)}}{\Delta + \gamma \cdot (1 + C_d \cdot u_2)} \quad (4)$$

where E_r : is the reference crop evaporation or reference evaporation (mm d^{-1}), Δ : is the slope of the saturation vapour pressure-temperature curve ($\text{kPa } ^\circ\text{C}^{-1}$), R_n : is the net radiation at the crop surface ($\text{MJ m}^{-2} \text{d}^{-1}$), G : is the soil heat flux density at the soil surface ($\text{MJ m}^{-2} \text{d}^{-1}$), γ : is the psychrometric constant ($\text{kPa } ^\circ\text{C}^{-1}$), u_2 : is the wind speed at 2 m height above the soil surface (m s^{-1}), e_s : is the saturation vapour pressure (kPa), e_a : is the actual vapour pressure (kPa), T_{mean} : is the mean daily air temperature ($^\circ\text{C}$), C_n and C_d : are constants, which vary according to the time step and the reference crop type and describe the bulk surface resistance and aerodynamic roughness. Eq.4 can be applied for two types of reference crop, this study focuses on the short reference crop (ASCE-short), which corresponds to clipped grass of 12 cm height and surface resistance of 70 s m^{-1} where the constants C_n and C_d have the values 900 and 0.34, respectively (Allen et al., 2005).

The derivation of a correction factor for Eq.1 using as a benchmark the monthly values of Eq.4 (same to FAO-56) is performed based on the same procedure proposed by Aschonitis et al. (2017) that has been used before for developing partial weighted annual correction factors for Priestley-Taylor and Hargreaves-Samani methods. The procedure starts with the derivation of the monthly correction coefficient $c_{th,i}$ for each month i directly by dividing Eq.4 by Eq.1 of each month. Applying this procedure, twelve values of monthly $c_{th,i}$ are produced. The 12 monthly $c_{th,i}$ coefficients are then used to build mean annual coefficients. As it was mentioned in Aschonitis et al. (2017), the efficiency of mean annual correction factors is mainly associated with the fact that they are corresponding better for larger evaporation levels (i.e., the values of E_r during summer/hot months) and not the smaller values where the absolute errors ($e_i = E_{ri} - E_{pi}$) are smaller. In that scope, the use of weighted annual averages based on the monthly $c_{th,i}$ coefficients are estimated considering the participation weight of each month in the annual E_r ; the weight of each month was calculated by dividing the reference evaporation of each month into the annual reference evaporation.

Under cold conditions, reference evaporation is very low and sensitive to climate parameters (e.g., wind speed) a fact which means that the aforementioned division can lead to unrealistic monthly coefficients $c_{th,i}$ that may cause a negative impact on the averaged coefficients and led to nonrealistic coefficients (one order of magnitude deviation from 1). The solution of that situation came by setting a low limit of E_p and E_r before the inclusion of their $c_{th,i}$ in the weighted average estimations. In order to set this limit, a preliminary analysis was done by a trial-and-error method, this methodology led to the rejection of values lower than 1.5 millimeter per day which is equal to 45 millimeters for the whole month.

The derivation of the partial weighted average is based on monthly $c_{th,i}$ values after excluding the $c_{th,i}$ values of those months with E_r and/or $E_p \leq 45 \text{ mm month}^{-1}$:

$$c_{th,i} = \frac{E_{ri}}{E_{pi}} \quad (5)$$

$$\text{If } E_{ri} > 45 \text{ mm month}^{-1} \text{ then } F_{ri} = 1 \text{ else } = 0 \quad (6)$$

$$\text{If } E_{pi} > 45 \text{ mm month}^{-1} \text{ then } F_{mi} = 1 \text{ else } = 0 \quad (7)$$

$$E_{ri}^{adj} = E_{ri} \cdot F_{ri} \cdot F_{mi} \quad (8)$$

$$AE_r^{adj} = \sum_{i=1}^{12} (E_{ri}^{adj}) \quad (9)$$

$$C_{th} = \sum_{i=1}^{12} \left(\frac{E_{ri}^{adj}}{AE_r^{adj}} \cdot c_{th,i} \right) \quad (10)$$

where $c_{th,i}$: is the monthly correction coefficient, F_{ri} and F_{mi} : are corresponding to Eq.1 and Eq.4 and are having a binary form in order to apply a filtering on the evaporation values, E_{ri}^{adj} : is the adjusted monthly value of E_{ri} from Eq.4, AE_r^{adj} : is the sum of the monthly E_{ri}^{adj} adjusted values, C_{th} : annual partial weighted average of the monthly $c_{th,i}$ coefficients and i : is each month's index

Considering the above, the final corrected Thornthwaite formula for monthly calculations is given by the following equation:

$$E_{psi} = C_{th} \cdot E_{pi} \quad (11)$$

where E_{psi} : is the corrected temperature-based short crop evaporation (mm month⁻¹) of each month i .

The above led to the adjustment of the annual C_{th} (Eq.10) for every location during the period 1950-2000 on the globe based on mean monthly E_r and E_p taking:

- the gridded mean monthly data for the temperature Hijmans et al. (2005) that were further used to estimate the mean monthly gridded original Thornthwaite E_p (Eq.1) for the period 1950-2000 (in the form of 12 raster datasets of E_p for each month),
- the respective mean monthly grids of E_r based on ASCE-standardized method (Eq.1) (Aschonitis et al. (2017)) (in the form of 12 raster datasets of E_r for each month).

2.1.2. Variation of Thornthwaite correction factor in major climate groups of Köppen-Geiger climate classification

Aiming to investigate variations of the final values in the global map of the C_{th} factor concerning climate, the major groups of Köppen-Geiger climate classification were used. A total number of 114,065 randomly generated sampling points, with the density of 1000 stations per million km², was used to extract the C_{th} factor and the 12 mean monthly values of T and P from Hijmans et al. (2005) project. Using the monthly average precipitation and temperature, the Köppen-Geiger climate classification was assessed for each sampling position based on the criteria of Table 2.1 obtained from Peel et al. (2007). The C_{th} values were divided into A, B, C, D, E groups of Köppen-Geiger, and their distribution within each group was analysed using a faction to investigate the distribution of the correction factor. Due to Bernardo (2005), the implementation of the module *p.interval* which is part of the *LaplacesDemon* in R statistic language, is able also to reveal the modality of the distribution and apply specific confidence level for the sample (e.g., 2.5 to 97.5 %). The aforementioned climate classification was followed as it was described from the paper of Peel et. al 2007.

2.1.3. Validation of C_{th} based on stations data

The validation procedure with the data of the 525 stations was performed by comparing the mean monthly and the mean annual values of E_r of ASCE (Eq.4) versus the original E_p (Eq.1) and versus the modified E_{ps} Thornthwaite formula (Eq.11) for short reference crop taking into account the annual partial weighted average coefficients C_{th} . The validation was made separately for each database of stations (ECAD, AGBM, CIMIS) but also all together using the following five statistical criteria were applied to the results to assess their accuracy.

$$MAE = \frac{1}{N} \sum_{i=1}^N |S_i - O_i| \quad (12)$$

$$ME = \frac{1}{N} \sum_{i=1}^N (S_i - O_i) \quad (13)$$

$$RMSE = \sqrt{\frac{1}{N} \sum_{i=1}^N (S_i - O_i)^2} \quad (14)$$

$$R_{Sqr} = \left[\frac{\sum_{i=1}^N (O_i - \bar{O}_i)(S_i - \bar{S}_i)}{\sqrt{\sum_{i=1}^N (O_i - \bar{O}_i)^2 \sum_{i=1}^N (S_i - \bar{S}_i)^2}} \right]^2 \quad (15)$$

$$d = 1 - \frac{\sum_{i=1}^N (S_i - O_i)^2}{\sum_{i=1}^N (|S_i - \bar{O}_i| + |O_i - \bar{O}_i|)^2} \quad (16)$$

where *MAE*: is the mean absolute error (mm month⁻¹), *ME*: is the mean error (mm month⁻¹), *RMSE*: is the root mean square error (mm month⁻¹), *R_{Sqr}*: is the coefficient of determination (-) and *d*: is the index of agreement (-), *O*: is the observed value (i.e., *E_r*) (mm month⁻¹), *S*: is the simulated value from the model (i.e., *E_p* or *E_{ps}*) (mm month⁻¹), *N*: is the number of observations, *i*: is the subscript referred to each observation.

Table 2.1: Description and characteristics of statistical criteria

Statistical criterion	Abbreviation	Range	Value of perfect fit
Mean Absolute Error	<i>MAE</i>	0 and +∞	0
Mean Error	<i>ME</i>	-∞ and +∞	0
Root Mean Squared Error	<i>RMSE</i>	0 and +∞	0
<i>R_{Sqr}</i> statistic (Coefficient of Determination)	<i>R_{Sqr}</i>	0 and 1	1
Index of Agreement	<i>d</i>	-∞ and 1	1

2.1.4. Evaluation of *C_{th}* use in aridity and aridity/humidity indices based on stations data

The role of the new corrected version of Thornthwaite (Eq.11) as an internal parameter of aridity indices was also evaluated against the original method (Eq.1). For this purpose, the *A_{IUNEP}* (UNEP, 1997) and *A_{ITH}* (Thornthwaite, 1948) climate/aridity indices were used. The two indices estimated based on the *E_r* of ASCE (Eq.4) were used as a benchmark in order to compare the respective indices calculated with the original Thornthwaite (Eq.1) and the corrected one (Eq.11) for the stations' data. The comparative analysis was performed using the same metrics of Eqs.12-16 and through % similarity comparisons in the derivation of aridity code classes. The *A_{IUNEP}* is the simplest method for hydroclimatic analysis and it is given by the following equation:

$$A_{IUNEP} = \frac{P_y}{E_y} \quad (17)$$

where *P_y*: mean precipitation (mm y⁻¹) and *E_y*: mean annual potential evaporation (mm y⁻¹).

Applying the Eq.16, the characterization of the area is corresponding to five classes (UNEP, 1997; Cherlet, 2018):

- $0.05 > A_{IUNEP}$ → Hyper-arid
- $0.05 \leq A_{IUNEP} < 0.2$ → Arid
- $0.2 \leq A_{IUNEP} < 0.5$ → Semi-arid
- $0.5 \leq A_{IUNEP} < 0.65$ → Dry subhumid
- $0.65 \leq A_{IUNEP}$ → Humid

It is also popular to merge the classes > 0.65 to a humid one. The UNEP index does not consider the effect of seasonal variation of precipitation and potential evaporation. The A_{ITH} aridity – humidity index is calculated as follows:

$$S = \sum_{i=1}^{12} (P_i - E_i) \quad \text{and} \quad D = \sum_{i=1}^{12} (E_i - P_i) \quad (18a,b)$$

$$A_{ITH} = 100 \cdot \frac{S - 0.6D}{E_y} \quad (19)$$

where S (mm y^{-1}) is the positive difference between evaporation and precipitation ($P_i - E_i > 0$, (if negative $S = 0$), D (mm y^{-1}), is the positive difference between precipitation and evaporation ($P_i - E_i > 0$ (if negative $D = 0$)).

The various climatic types according to A_{ITH} values are the following:

- $-60 > A_{ITH}$ → Hyper-arid
- $-60 \leq A_{ITH} < -40$ → Arid
- $-40 \leq A_{ITH} < -20$ → Semi-arid
- $-20 \leq A_{ITH} < 0$ → Dry sub-humid
- $0 \leq A_{ITH} < 20$ → Moist sub-humid
- $20 \leq A_{ITH} < 40$ → Humid
- $40 \leq A_{ITH} < 60$ → Humid
- $60 \leq A_{ITH} < 80$ → Humid
- $80 \leq A_{ITH} < 100$ → Humid
- $100 \leq A_{ITH}$ → Hyper-humid

2.2. Data

In this study, global gridded data from two databases were used. The first [Hijmans et al. \(2005\)](#) supplies open-source gridded data of average precipitation P and temperature T per month for the period 1950-2000 (WorldClim version 1.2) with a resolution of ~ 1 km grid resolution. The described data is presented in the [Fig. 2.2a, b](#). The second database is the one of [Aschonitis et al. \(2017\)](#), which provides gridded data of mean monthly reference evaporation E_r of the period 1950-2000 at 30 arc-sec ($\sim 1 \times 1$ km) spatial resolution ([Fig. 2.2c](#)). The method used for estimating E_r is the one of ASCE-standardized method (former FAO-56), which estimates reference evaporation from short clipped grass ([Allen et al., 2005](#)). The database of E_r was built using temperature from the first raster of [Hijmans et al. \(2005\)](#) and for this reason, the two gridded databases are compatible for being used and combined in the common analysis.

For the validation of the correction factors, it was necessary to compare its performance with in-situ data; the use of meteorological data obtained from ground stations was important. The network of California, USA (CIMIS) was the first option based on the geometry and the high density of the network. The advantage of the specific area in USA is its climate variability and the rich landscape. In total 60 stations ([Fig. 2.1a](#)) were used from CIMIS database that has at least 15 years of observations with a significant part of their observations after 2000 (some stations, that do not follow the first rule were selected due to their special climate Köppen class or the high altitude of their location). From the total stations, it has been excluded these that are located in extreme climates or/and high elevation.

The large variability that also presenting in the Australian continent (from tropical to desert) such as the well distributed and enough dense network, made it adequate to be included in the study. The second stations' network is the AGBM and consists of 80 stations ([Fig. 2.1b](#)), that have at least 15 years of observations with a significant part of their observations after 2000 (the same filtering that was done for the CIMIS has been done for AGBM also).

The third database is the ECAD database (European Climate Assessment & Database, <https://www.ecad.eu>). This database is a network that contains more than 20,000 stations throughout Europe and provides daily observations of climatological parameters. In this study, a final number of 385 stations (Fig. 2.1c) was selected because they contained complete data of precipitation, temperature, solar radiation, relative humidity and wind speed for a period of at least 20 years (with a significant part of their observations after 2000). The total number of stations used in the study from the three databases is 525 (Table S1).

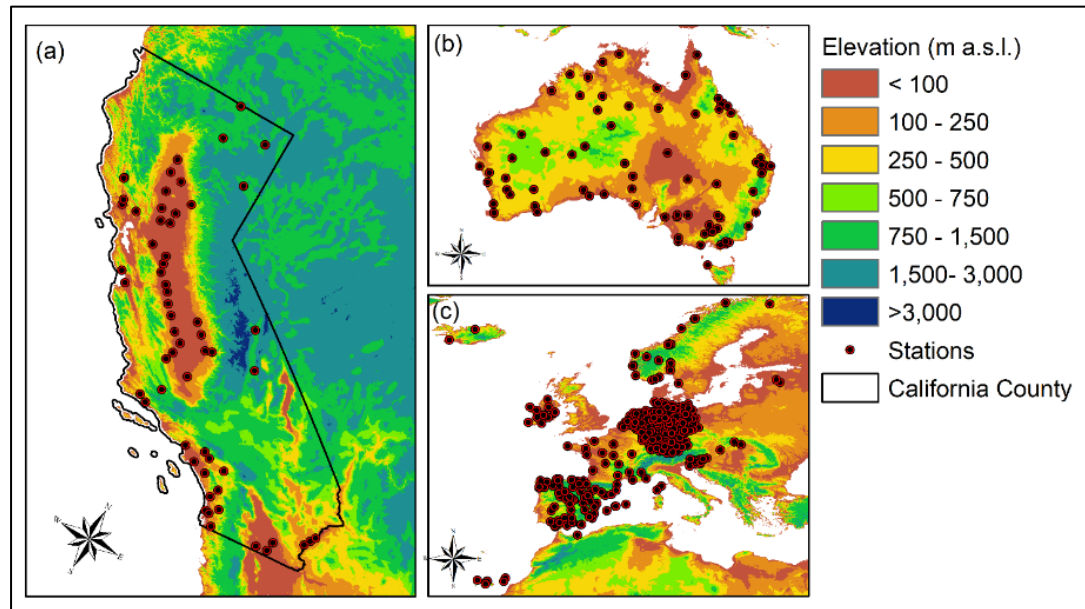


Figure 2.1: (a) 60 stations of California from CIMIS database, (b) 80 stations of Australia from AGBM database, and (c) 385 stations of Europe from ECAD database.

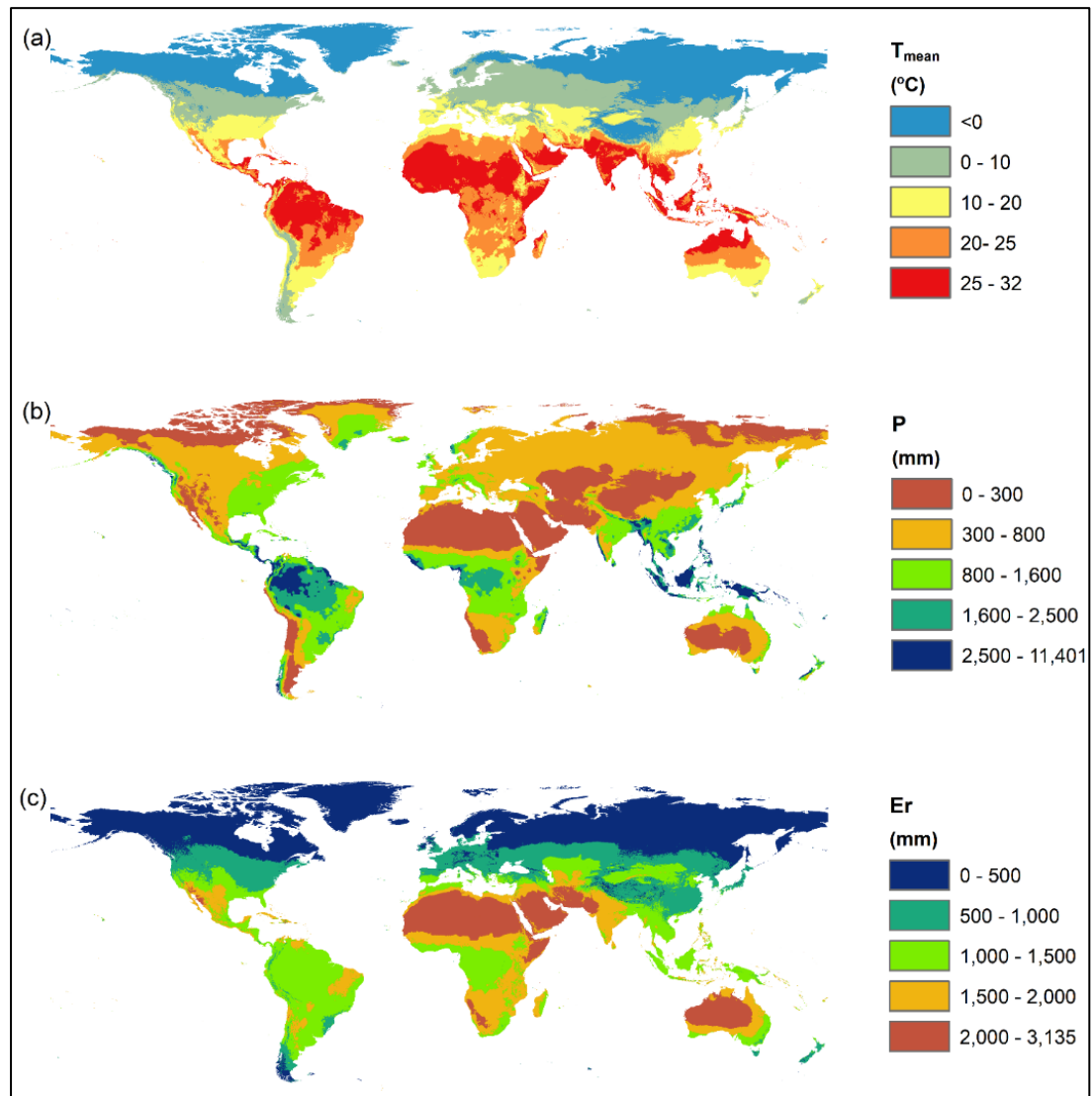


Figure 2.2: (a) Annual average temperature between 1950 and 2000 (Hijmans et al., 2005), (b) Annual average precipitation for the period of 1950-2000 (Hijmans et al., 2005), (c) Annual average reference evaporation of ASCE-standardized method for short reference crop between 1950 and 2000 (Aschonitis et al., 2017).

3

Results

3.1. Derivation of the C_{th} correction factors and analysis of its variation in major Köppen-Geiger groups

The global map of the C_{th} correction factor was developed following the procedure described in Section 2.1 and it is given in Fig.3.1a. The C_{th} map is given together with the additional map of 114,065 randomly selected sampling points providing information about their Köppen-Geiger climate classification (Fig.3.1b), which was identified following the criteria of Table 2.1 using Hijmans et al. (2005) database. These points were used to evaluate the variation of C_{th} values inside the major groups as described in section 2.1.2. The HPD distributions of C_{th} values separately for each major climate group but also all groups together are given in Fig.3.2a-f, while their respective statistics are given in Table 3.1. Places with $C_{th} = 0$ due to extreme cold (T_{mean} always < 0) were not included in the sampling points. According to Table 3.1, the five major Köppen-Geiger groups are ordered as follows $B > C > A > D > E$ considering the magnitude of their mean, median, mode C_{th} values.

Considering C_{th} as an indirect metric of error, it is observed that there are regions in the globe mostly belonging to the B group where the original formula of Thornthwaite greatly underestimates reference evaporation (E_r can be more than double from E_p). On the other hand, there are regions mostly belonging to the D and E groups where the original formula of Thornthwaite greatly overestimates reference evaporation (E_p can be more than double from E_r). In general, E_p overestimates reference evaporation in environments of high humidity and low water vapour deficit, while it underestimates it in dry environments with high water vapour deficit. Finally, E_p is showing the most symmetric behaviour at a global scale considering the statistics of all Köppen-Geiger groups of Table 3.1. Finally, it is very interesting to investigate the behaviour of C_{th} through the regions that Thornthwaite originally used for the derivation of the Eq.1. Due to Willmott et al. (1985), Thornthwaite used lysimeters at the East part of the U.S., the value of C_{th} in the aforementioned areas is close to neutral (0.9 – 1.1).

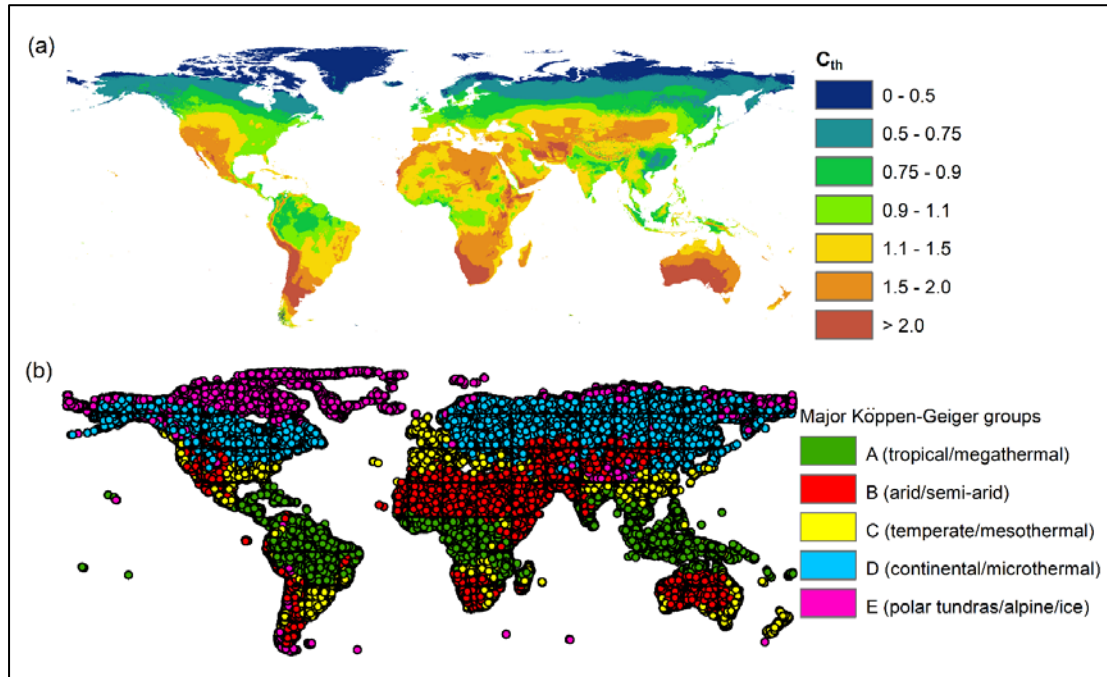


Figure 3.1: (a) Global map of the annual partial weighted average C_{th} factors, (b) Köppen-Geiger climate classification map, (c) sampling points distribution.

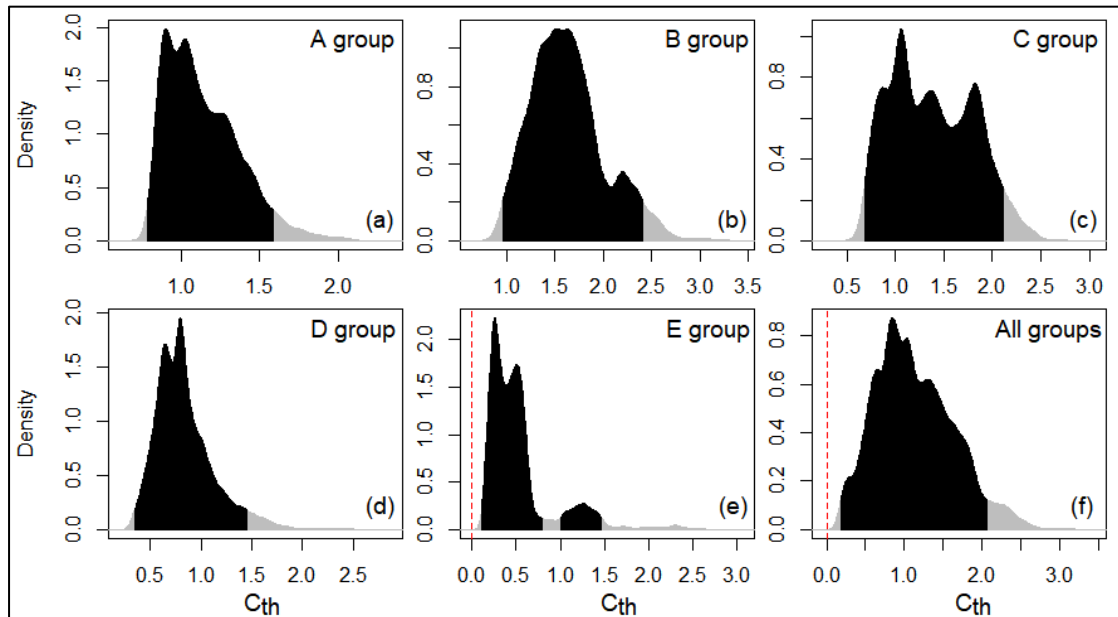


Figure 3.2: HPD distributions of C_{th} per each major Köppen-Geiger group and f) for all Köppen-Geiger groups (excluding places where $C_{th}=0$)

Table 3.1: General statistics and 2.5% and 97.5% thresholds of HPDs given in Fig.4 for the C_{th} values of each major Köppen-Geiger group and all groups.

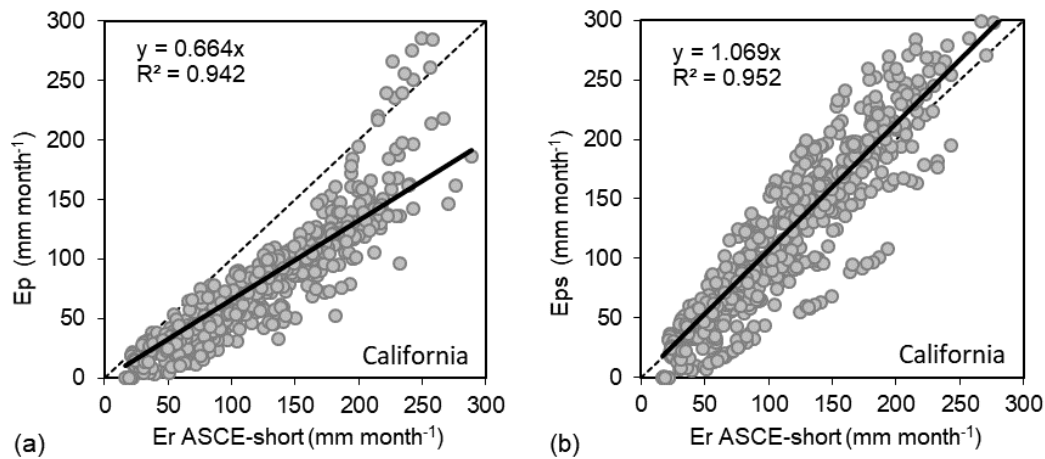
Parameter	Köppen-Geiger Groups					All Groups
	A	B	C	D	E	
Number of samples	18151	31179	12992	40785	10958	114065
Mean	1.14	1.63	1.38	0.84	0.54	1.14
Median	1.09	1.59	1.34	0.79	0.43	1.07

Parameter	Köppen-Geiger Groups					All Groups
	A	B	C	D	E	
Mode	0.90	1.66	1.05	0.80	0.24	0.80
Minimum	0.70	0.76	0.43	0.28	0.09	0.09
Maximum	2.25	3.33	2.89	2.80	2.98	3.33
2.5% HPD threshold*	0.78	0.93	0.69	0.33	0.13	0.17
97.5% HPD threshold*	1.58	2.38	2.11	1.43	1.37	2.07
Standard Error	0.002	0.002	0.004	0.001	0.004	0.001
Standard Deviation	0.234	0.385	0.425	0.292	0.394	0.506
Sample Variance	0.055	0.148	0.180	0.085	0.155	0.256

*Represent the central 95% of HPD even for the HPD of Fig.3.2e. The two multimodal intervals presented in Fig.3.2e are defined by these two ranges, respectively: 0.1-0.8 and 1.0-1.47.

3.2. Validation of the C_{th} correction factors

The validation of the derived C_{th} factors (Fig.3.1a) was performed for each of the three datasets of stations (California-CIMIS, Australia-AGBM, Europe-ECAD), separately, by comparing in 1:1 plots the performance of mean monthly values of original Thornthwaite E_p (Eq.1) and mean monthly E_{ps} (Eq.11) versus the benchmark values of E_r (Eq.4) (Fig.3.3a-f). The same comparisons were also performed using the mean annual values of the respective methods (Fig.3.4a-f). The statistical criteria (Eqs.12-16) for both monthly and annual comparisons for each one of the three datasets of stations are given in Table 3.2. The respective monthly and annual comparisons after merging all the stations from the three datasets are also presented in Fig.3.5a-d. From the results shown in Figs.3.3, 3.4, 3.5 and Table 3.2, it is observed that E_{ps} much better performance compared to the original Thornthwaite formula E_p in all cases providing not only better monthly but also better annual reference evaporation estimations that approximate the values of ASCE for short reference grass.



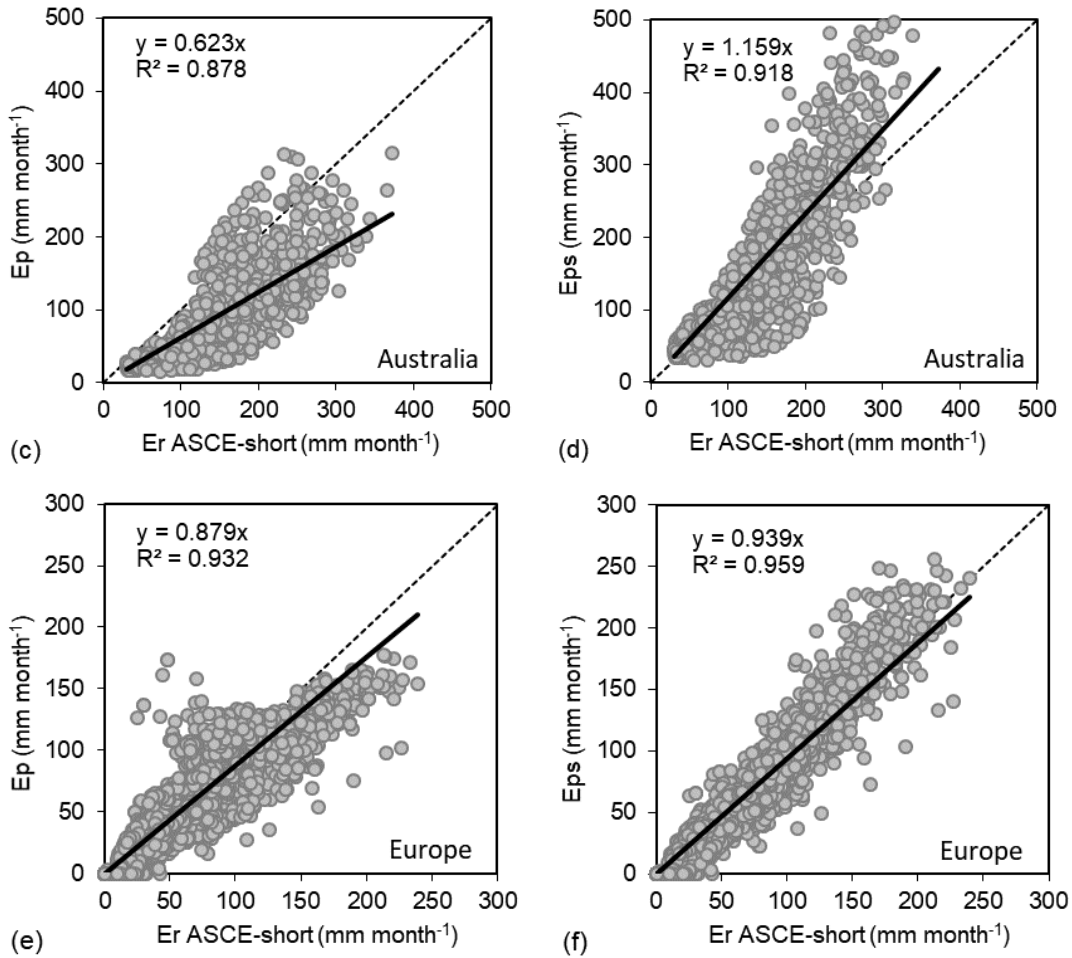
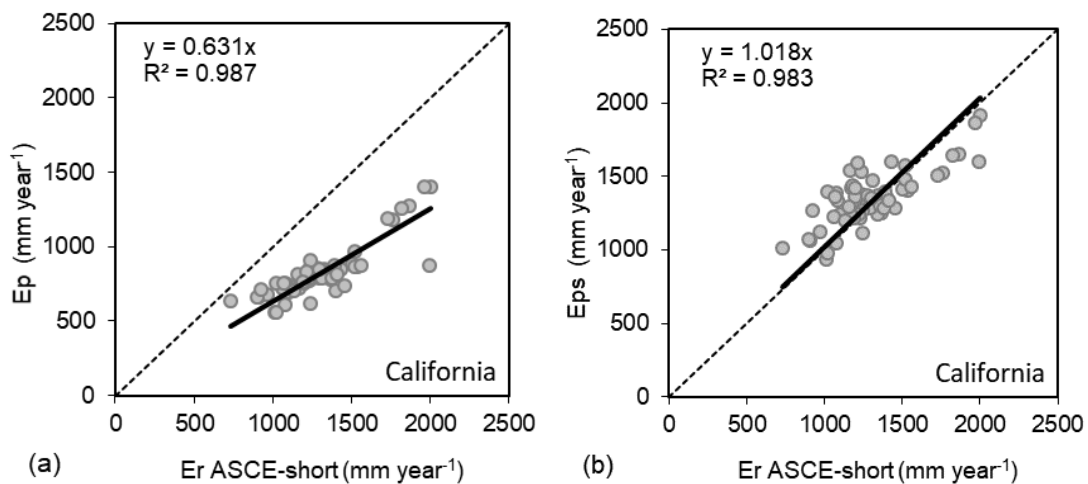


Figure 3.3: *Left side:* 1:1 plots of mean monthly E_p (Eq.1) versus mean monthly E_r (Eq.4) (a) for 60 CIMIS stations of California, (c) for 80 AGBM stations of Australia and (e) for 385 ECAD stations of Europe, and *Right side:* 1:1 plots of mean monthly E_{ps} (Eq.11) versus mean monthly E_r (Eq.4) (b) for 60 CIMIS stations of California, (d) for 80 AGBM stations of Australia and (f) for 385 ECAD stations of Europe.



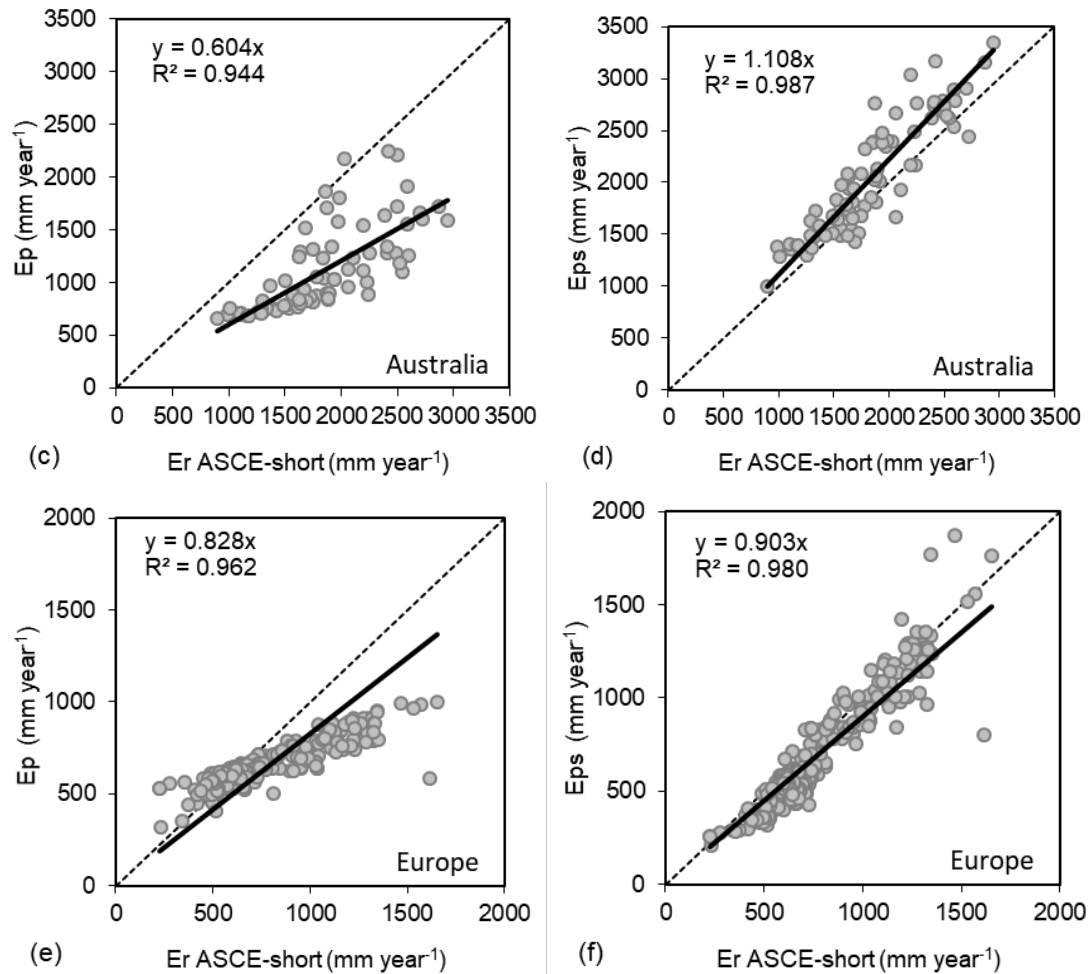


Figure 3.4: *Left side:* 1:1 plots of mean annual E_p (Eq.1) versus mean annual E_r (Eq.4) (a) for 60 CIMIS stations of California, (c) for 80 AGBM stations of Australia and (e) for 385 ECAD stations of Europe, and *Right side:* 1:1 plots of mean annual E_{ps} (Eq.11) versus mean annual E_r (Eq.4) (b) for 60 CIMIS stations of California, (d) for 80 AGBM stations of Australia and (f) for 385 ECAD stations of Europe.

Table 3.2: Statistical metrics (Eqs.12-16) for the comparisons between E_p vs. E_r and E_{ps} vs. E_r for CIMIS-California, AGBM-Australia and ECAD-Europe stations for (a) mean monthly and (b) mean annual analysis.

	California		Australia		Europe	
	E_p vs. E_r	E_{ps} vs. E_r	E_p vs. E_r	E_{ps} vs. E_r	E_p vs. E_r	E_{ps} vs. E_r
(a) Metrics based on mean monthly values						
No. Records [-]	720	720	960	960	4620	4620
MAE [mm month ⁻¹]	40.3	22.6	64.6	45.2	14.5	11.9
ME [mm month ⁻¹]	-39.7	4.1	-60.5	17.3	-7.4	-6.9
RMSE [mm month ⁻¹]	46.4	31.0	74.2	63.7	20.1	15.3
R_{Sqr} [-]	0.852	0.858	0.624	0.746	0.824	0.919
d [-]	0.847	0.948	0.743	0.867	0.945	0.972
(b) Metrics based on mean annual values						
No. Records [-]	60	60	80	80	385	385
MAE [mm month ⁻¹]	476.2	142.1	730.5	256.8	116.6	101.6
ME [mm month ⁻¹]	-476.2	49.8	-726.5	208.0	-89.3	-83.1
RMSE [mm month ⁻¹]	500.1	177.9	800.2	317.0	184.7	126.0
R_{Sqr} [-]	0.717	0.603	0.526	0.812	0.785	0.879

d [-]	California		Australia		Europe	
	E_p vs. E_r	E_{ps} vs. E_r	E_p vs. E_r	E_{ps} vs. E_r	E_p vs. E_r	E_{ps} vs. E_r
	0.501	0.845	0.571	0.906	0.728	0.94

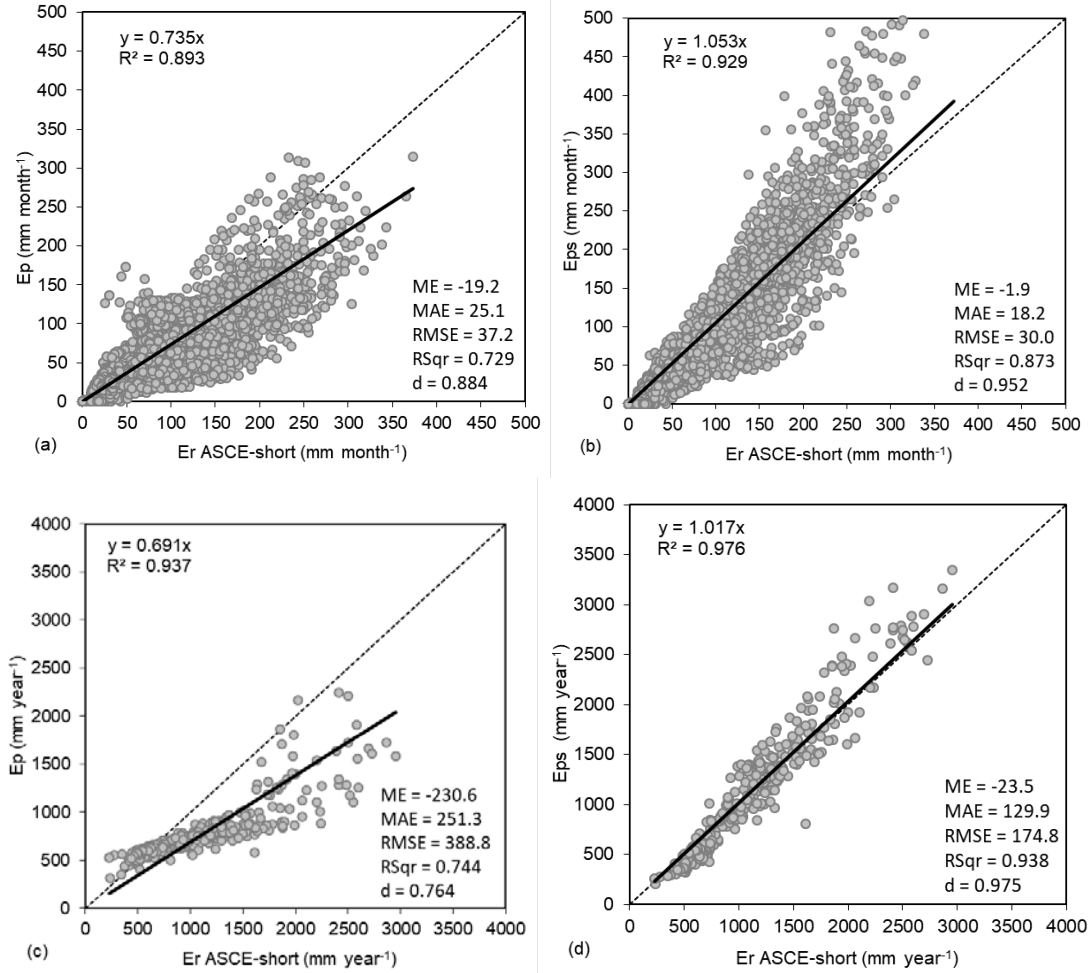


Figure 3.5: 1:1 plots of (a) mean monthly E_p (Eq.1) versus mean monthly E_r (Eq.4), (b) mean monthly E_{ps} (Eq.11) versus mean monthly E_r (Eq.4), (c) mean annual E_p (Eq.1) versus annual monthly E_r (Eq.4), (d) mean annual E_{ps} (Eq.11) versus annual monthly E_r (Eq.4), using the data of all 525 stations from the three databases of CIMIS, AGBM, ECAD.

3.3. Evaluating the use of C_{th} factor in aridity indices

The use of derived C_{th} factors (Fig.3.1a) in A_{IUNEP} and A_{ITH} aridity indices was evaluated considering all 525 stations (California-CIMIS, Australia-AGBM, Europe-ECAD) that were included in the validation procedure of the previous analysis. The evaluation was performed both by using statistical metrics (Eqs.12-16) for comparing the values of the indices or by converting their values to aridity classes in order to compare their correspondence. The statistical metrics of Eqs.12-16 for the evaluation between E_p vs. E_r and E_{ps} vs. E_r when they are applied in the A_{IUNEP} and A_{ITH} aridity indices considering only non-humid or humid classes based on the data of all 525 stations are given in Table 3.3.

For the case of A_{IUNEP} , the analysis was made by comparing the performance of the index when estimated using the original Thornthwaite E_p (Eq.1) and using the mean monthly E_{ps} (Eq.11) versus the A_{IUNEP} benchmark values estimated using E_r (Eq.4) in 1:1 log-log plots.

The results of the analysis are given in Figs. 3.6a,b for E_p and E_{ps} , respectively. The 1:1 plots were visualized with log-transformed axes in order to optimize the visualization of high A_{IUNEP} deviations based on E_p for A_{IUNEP} values < 0.65 , which is the minimum threshold value of the last Humid class of A_{IUNEP} classification. The visual comparison clearly shows that E_{ps} outperforms the E_p in the range of 0-0.65 where there are all the divisions of A_{IUNEP} classes (Table 3.3). Considering the full set of 5 classes of the A_{IUNEP} index and the complete set of stations, the A_{IUNEP} of E_{ps} provided 93% of identical codes with the A_{IUNEP} of E_r , while A_{IUNEP} of E_p provided 76% of identical codes. For the case of A_{ITH} , the analysis was made in the same way as A_{IUNEP} . In order to visualize the negative values of A_{ITH} in 1:1 log-log plots, a constant value was added (+70) to all the A_{ITH} values. The results of the analysis are given in Figs. 3.7a,b for E_p and E_{ps} , respectively. The 1:1 plots were again visualized with log-transformed axes in order to optimize the visualization of high A_{ITH} deviations based on E_p for A_{ITH} values < 20 , which is the minimum threshold value of the Humid B and A classes of A_{ITH} classification. The comparison again shows that E_{ps} outperforms the E_p in the A_{ITH} range of < 20 (Table 3.3). The A_{ITH} of E_{ps} provided 58% of identical codes, while the A_{ITH} of E_p provided 52% of identical codes with the A_{ITH} of E_r according to the 10 aridity-humidity classes of the index.

Table 3.3 verifies the better performance of E_{ps} compared to E_p in both A_{IUNEP} and A_{ITH} aridity indices for the non-humid classes. On the other hand, the statistics showed that E_p showed better performance in both A_{IUNEP} and A_{ITH} aridity indices for humid classes, but this result is of less importance and not so robust for the following reasons:

- In the case of $A_{IUNEP} > 0.65$, there is only one Humid class and thus there is no point to compare the performance of E_p and E_{ps} in A_{IUNEP} from a statistical point of view since their values will always lead to the same classification code/characterization (i.e. Humid).
- In the case of $A_{ITH} > 20$, the detailed division of five humid classes (B1, B2, B3, B4, A) provided by A_{ITH} was proposed for the alternative use of the index as “humidity index” (Thornthwaite, 1948). Merging the B and A classes to one Humid class, as in the case of A_{IUNEP} , the successful identical codes are raised to 76% for E_{ps} and 63% for E_p indicating in both cases (merging or no merging of humid A_{ITH} classes) the better performance of E_{ps} compared to E_p despite the worst statistical metrics.

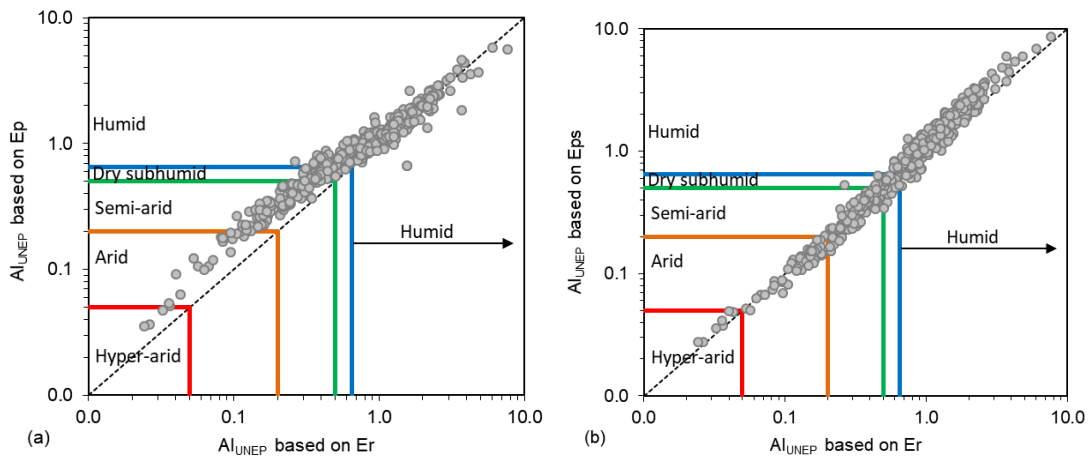


Figure 3.6: 1:1 log-log plots of (a) A_{IUNEP} using mean monthly E_p (Eq.1) versus A_{IUNEP} using mean monthly E_r (Eq.4), (b) A_{IUNEP} using mean monthly E_{ps} (Eq.11) versus mean monthly E_r (Eq.4) using the data of all 525 stations from the three databases of CIMIS, AGBM, ECAD.

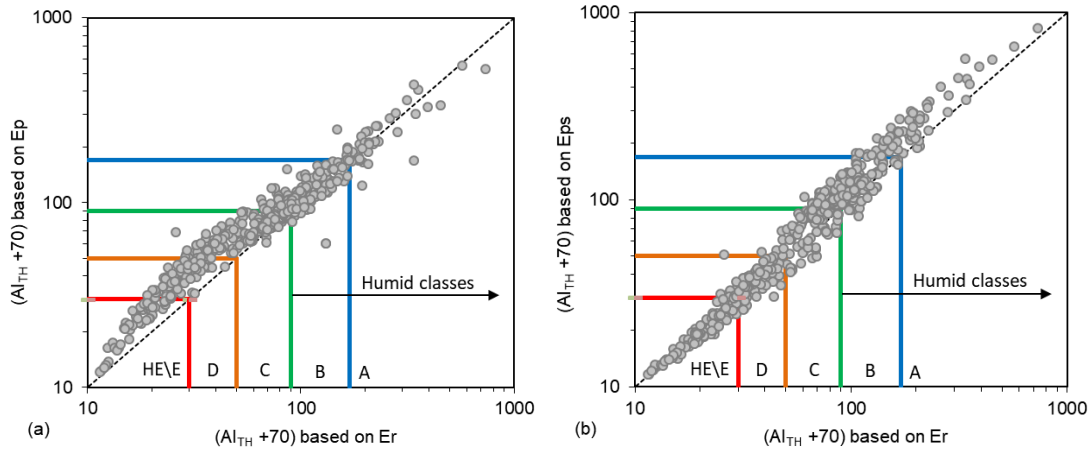
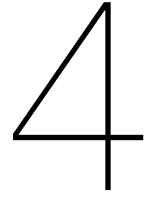


Figure 3.7: 1:1 log-log plots of (a) A_{ITH} using mean monthly E_p (Eq.1) versus A_{ITH} using mean monthly E_r (Eq.4), (b) A_{ITH} using mean monthly E_{ps} (Eq.11) versus mean monthly A_{ITH} (Eq.4) using the data of all 525 stations from the three databases of CIMIS, AGBM, ECAD.

Table 3.3: Statistical metrics (Eqs.12-16) for the evaluation between E_p vs. E_r and E_{ps} vs. E_r when they are applied in the (a) A_{IUNEP} and (b) A_{ITH} aridity indices considering only non-humid or humid classes based on the data of all 525 stations from the three databases of CIMIS, AGBM, ECAD.

	E_p vs. E_r	E_{ps} vs. E_r	E_p vs. E_r	E_{ps} vs. E_r
(a)	$A_{IUNEP} \leq 0.65$ (non-humid)		$A_{IUNEP} > 0.65$ (humid)	
No. stations	197	197	328	328
MAE	0.169	0.036	0.151	0.264
ME	0.169	0.003	0.035	0.233
RMSE	0.194	0.056	0.264	0.376
R_{Sqr}	0.867	0.893	0.875	0.932
d	0.773	0.969	0.963	0.950
(b)	$A_{ITH} \leq 20$ (non-humid)		$A_{ITH} > 20$ (humid)	
No. stations	257	257	268	268
MAE	12.8	6.3	14.9	26.7
ME	12.7	3.6	3.0	24.2
RMSE	15.1	10.0	26.6	39.4
R_{Sqr}	0.842	0.882	0.872	0.928
d	0.855	0.939	0.962	0.945



Discussion

4.1. The validity of the derived C_{th} of 1950-2000 for periods after 2000

The calibration of local C_{th} factors at a global scale was performed using the mean monthly grid datasets for the period of 1950-2000 doing the assumption of relevant stable climate, on the other hand, the procedure of the validation was performed using stations data from California and Australia that are expanded up to 2016 and data from Europe that are expanded up to 2020 (Table S1). The reasons for choosing the grid datasets for calibration of C_{th} factors are the following:

- They are in the form of high-resolution grids, which have been developed using interpolation techniques that include the effects of latitude, longitude and elevation. These grids allow deriving more representative C_{th} values for every position even when weather stations do not locally exist.
- They cover a large period of time (i.e., 1950-2000) so they can provide more representative mean annual partial weighted average C_{th} values. The upper threshold of the year 2000 of these grids also allows the validation dataset of stations to be more valid since the larger part of their data is after 2000 and this reduces the possibility of having been used in grids' development.

On the other hand, several works have shown climate differences after 2000 (Hansen et al., 2010; McVicar et al., 2012a,b; Wild et al., 2013; Willet et al., 2014; Sun et al., 2017) a situation that is crucial for the performance and the validity of the correction factor C_{th} . The overall effect of all possible changes in climate parameters would impact the final estimated values of E_r , which uses the complete set of climate parameters, and of course the final estimated C_{th} values. In order to evaluate the impact of such possible changes after 2000, the mean monthly E_r values of the grids (from the calibration set of Aschonitis et al. 2017) (Fig.2.2c) and the derived C_{th} values of the period 1950-2000 (Fig.3.1a) were extracted from the positions of the stations used for validation. These values were compared with the respective values of E_r and C_{th} that were computed with the station's raw data and correspond to posterior periods after 2000. The results of this comparison are given in Fig.4.1a, b. From Fig.4.1a, it is observed a correlation of 98% between the E_r values from grids of 1950-2000 and the E_r values from the stations using data from posterior periods. Similarly, a correlation of 98% was observed in the respective values of C_{th} in Fig.4.1b. In the case of C_{th} , there is a distinct deviation of a station where the derived C_{th} of the period 1950-2000 (value equal to 1.37) is almost half from the one observed in the station (value equal to 2.44) using its raw data. The specific station is an exceptional case since it belongs to the Centro de Investigación Atmosférica de Izaña and it is at the top of a mountain at 2371 m above sea level in Tenerife island. The specific deviation is fully justified by the fact that the C_{th} value of the grid corresponds to an area of 1 km while the specific position of the station is at a very unique

position, which can be described as the most extreme position within this pixel. There are also 3 stations in Tenerife island where the derived C_{th} of 1950-2000 are in good correspondence with those estimated by the stations. The case of Izana station in Tenerife was the perfect example for triggering further investigation for the possible effects of scale in similar environments with extremely variable topography. Investigating the individual stations with the larger % deviation of E_{ps} from E_r and the respective topography of their surrounding environment, it was observed a similar case in the CIMIS database of California stations. In this case, the larger deviations were observed in stations, which are all concentrated in the coastline between Los Angeles and San Diego. The specific region is a narrow (~20-30 km) highly urbanized coastal zone of ~200 km, which is enclosed between the coastline and a hilly/mountainous zone. In the specific stations, the average of C_{th} values of the period 1950-2000 from the position of these stations was 1.85, while the average of C_{th} values using their raw data from the validation procedure was estimated at 1.46. Apart from the large topographic variation, another reason for the C_{th} differences in these stations could be the bias that has been removed by clearing extreme flagged meteorological parameters (e.g., wind speed) in the data of California stations of CIMIS database, which are probably associated with a hurricane or other extreme events in this region. The filtering by the [Sheffield et al. \(2006\)](#) of the measurements during usual extreme phenomena (e.g., hurricanes) in the area of California, is in question for the derivation of the wind grids that were used by [Aschonitis et al. \(2017\)](#) to build the E_r grids. This could justify the fact that the gridded C_{th} values of 1950-2000 at the positions of the stations are greater than the C_{th} values estimated by their raw data from CIMIS.

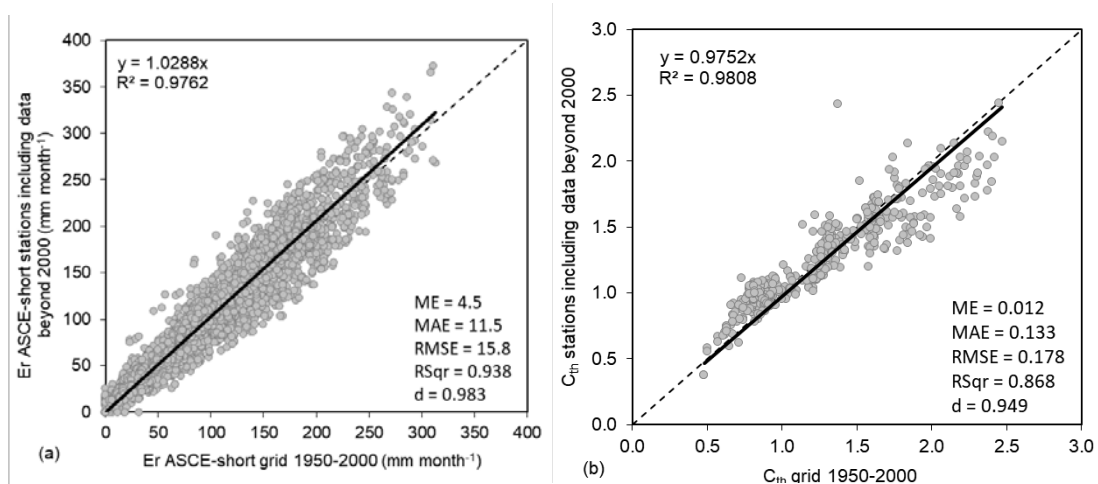


Figure 4.1: 1:1 plots of (a) mean monthly E_r of grids 1950-2000 ([Fig.2.2c](#)) vs. E_r of 525 stations raw data and (b) C_{th} of grids 1950-2000 ([Fig.3.1a](#)) vs. C_{th} of 525 stations estimated by their raw data. The values of grids correspond to the same positions of stations.

4.2. Scale effects on the accuracy of the derived C_{th}

An additional analysis based only on the stations of California was made in order to show that a regional mean value of C_{th} factors may present an equivalent or even better performance from the respective local high-resolution pixel values used in the validation procedure ([Figs.3.3b, 3.4b](#)) because it may counterbalance uncertainties by the possible variability of the climatic parameters in the wider area. The reason for such uncertainties could be rainfall, which may not present significant seasonal deviations or deviations from the expected annual values for a large region but may show different spatial patterns every year within the region affecting the accuracy of the coefficients. The results of the specific analysis are given in [Fig.4.2a,b](#) for the monthly and the annual results respectively using the same value of $C_{th}=1.66$ for all stations, which is the average value of all C_{th} factors of 1950-2000 from the positions of the stations. The results of this analysis showed that a regional average of C_{th} values

can lead to similar and in some cases better performance from the respective local high-resolution pixel values used in the validation procedure (Figs.3.3b, 3.4b)

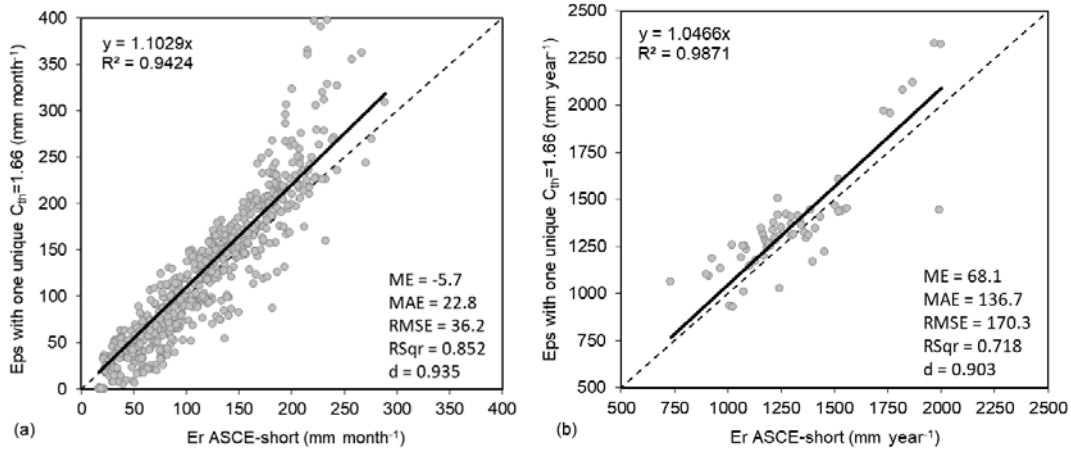


Figure 4.2: 1:1 plots of (a) of mean monthly E_{ps} (Eq.11) versus mean monthly E_r (Eq.4) and (b) of mean annual E_{ps} (Eq.11) versus mean annual E_r (Eq.4) for 60 CIMIS stations of California using the average value of their C_{th} values (i.e., equal to 1.66 for all stations) for the period 1950-2000.

4.3. Justifications about the methodology for deriving annual C_{th} correction factors based on partial weighted averages

The initial trials to derive annual correction factors C_{th} of this study were made using the average value of the twelve-monthly $c_{th,i}$ values. This procedure led to unreasonable values due to the extremely high values during winter. An example of this problem is given in the following Figure 4.3, which corresponds to a position close to Garda Lake in Italy (10.124° E, 45.45° N), where it can be seen that the monthly $c_{th,i}$ value of January is equal to 11.89. Based on the values of Figure 13, the annual average of monthly $c_{th,i}$ value for this location is equal to 2.4. Correcting the $E_{p,i}$ value of July with the factor 2.4 leads to $E_{r,i}$ equal to 338, which is 203 mm or 2.5 times larger than the respective $E_{r,i}$ of Figure 4.3. Thus, the specific procedure for deriving annual C_{th} factors was rejected.

A second approach was to use the 12 pairs of monthly E_r and E_p for each position on the grid to perform regression analysis based on the form $y = a \cdot x$ without intercept since reference evaporation $E_r = C_{th} \cdot E_p$. An example of the specific procedure based on the values of Figure 4.3 is given in Figure 4.4, where the annual C_{th} value was found equal to 0.98. The specific procedure provides annual C_{th} values, which are approaching better the higher evaporation months since the build of the methodology was aiming to reduce the error of the important/warm (in term of evaporation) months. Despite the fact that the specific procedure pays less attention to the monthly $c_{th,i}$ values of colder months, it was considered acceptable since most of the hydroclimatic applications require higher accuracy to the larger evaporation values rather to the lower ones. A similar approach was performed by Cristea et al. (2013) for deriving annual correction factors for the Priestley-Taylor method for 106 stations through the United States. The re-adjustment and the improvement of the Priestley Taylor equation based on the FAO-56 method for each specific station, only using the warmer semester of the year. The obtained optimized values of the correction factors for each station were then interpolated to produce a map of the Priestley-Taylor correction factors. For our study, the specific procedure was found to be extremely demanding in computing requirements since it was impossible to be performed pixel by pixel (777.6 million pixels) with a conventional computer unit for the whole globe using as input 24 rasters of extremely high resolution (~1 km) with a total size of ~70GB. In order to solve this problem, the method of partial weighted average (Eqs.5-10) was developed by Aschonitis et al. (2017), which provides similar results to the

regression analysis of $y = a \cdot x$ but allows to perform calculations step by step with a conventional computer unit. For the data of Figure 4.3, this method provided a C_{th} value equal to 0.99, which is almost similar to 0.98 of Figure 4.4. The specific method is also extremely efficient since it is not restricted only to the warmer semester or any other predefined periods like the case of Cristea et al. (2013) but controls all months one by one with the lower boundary of evaporation for 1.5 mm per day or 45 per month, which is more appropriate for global applications and especially for applications of high-resolution data giving the appropriate weight to the months with significant values of evaporation. The threshold of 45 mm month⁻¹ was derived empirically after analysing an extremely large number of positions in the globe (results not shown). This analysis showed that when monthly E_r was falling below 50-40 mm month⁻¹ then there was a steep increase of monthly $C_{th,i}$ (e.g. as in Figure 4.3). The reason for this increase is based on the fact that the original E_p formula is not including the combined effect of wind speed and vapour pressure deficit, which is much larger in colder months compared to the effect of temperature (Aschonitis et al., 2015, 2017). In the case where there is a location where all months show evaporation values below 45 mm month⁻¹ ($C_{th} = 0$ according to the procedure of Eqs.5-10), it is primarily suggested to use the non-zero C_{th} value of the closest location in the map of Figure 3.1a, or to use directly the original Thornthwaite without correction.

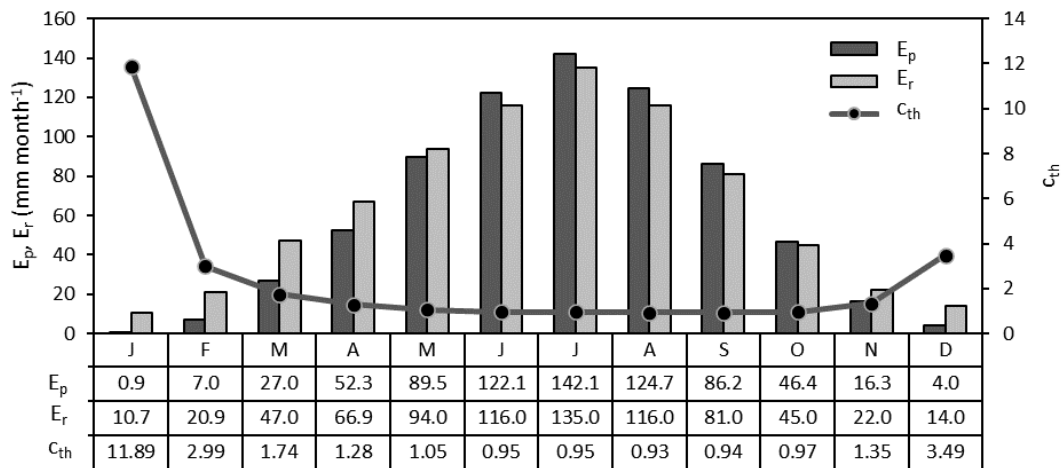


Figure 4.3: Monthly values of original Thornthwaite $E_{p,i}$ and ASCE $E_{r,i}$ method together with their respective monthly correction factors for a position close to Garda Lake in Italy (10.124° E, 45.45° N).

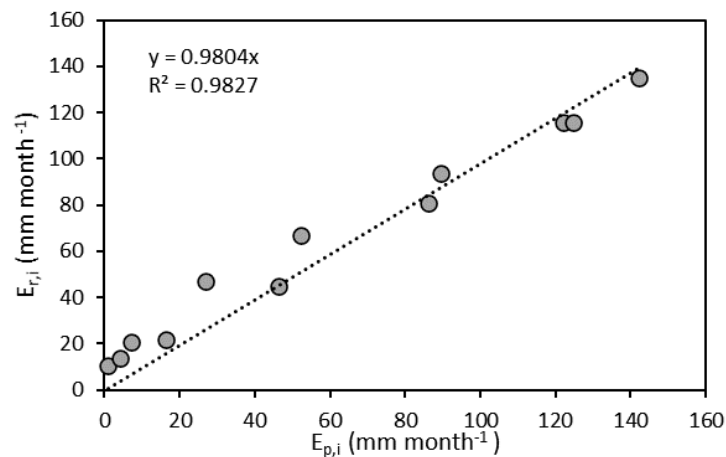


Figure 4.4: Simple linear regression analysis without intercept between monthly values of original Thornthwaite $E_{p,i}$ and ASCE $E_{r,i}$ from Figure 4.3.

5

Conclusions

A global grid of local correction factors for improving the performance of the temperature-based Thornthwaite evaporation method was built using gridded data covering the period 1950-2000. The method for developing the correction factors was based on partial weighted averages of their respective monthly average values, which were based on monthly ratios between the benchmark ASCE-standardized E_r method versus the original Thornthwaite E_p . This method led to annual values considering the amplitude of E_r is considering with more gravity to the monthly correction factors for the months with large E_r values, which are more important for irrigation, aridity and other water-associated procedures. The threshold of the study is also achieving to limit the estimation of unrealistic values c_{thi} that will impact a movement for the partial weighted correction factor. The values of correction factors extracted from the five major Köppen-Geiger groups (A, B, C, D, E) were investigated and showing the following order of magnitude $B > C > A > D > E$. The correction factors were validated using raw data from 525 stations of California, Australia and Europe that cover periods beyond 2000. The results showed that the corrections factors significantly improved the monthly and annual results of original Thornthwaite method E_p . The use of E_p with or without correction factors was also evaluated through the use in the aridity indices of Thornthwaite and UNEP versus the respective indices estimated based on the benchmark ASCE-standardized E_r . The results showed again that the correction factors significantly improved the performance of the indices compared to the original Thornthwaite method, especially in non-humid environments. Uncertainties in the values of correction factors were observed in regions of high topographic variability and a possible recommendation for such cases is the use of a regional average correction factor. The methods and results presented in this study and the limitations and unrealizabilities should be investigated further in future works, by focusing on: (a) the extent of the validation procedure in different areas, (b) assessment of the performance of other known empirical models that are using reduced parameters (c) use of p. w. a. method for recalibrating correction factors using the station or climate models' data of recent periods.

Bibliography

- Alexandris, S., Kerkides, P., & Liakatas, A. (2006). Daily reference evapotranspiration estimates by the “Copais” approach. *Agricultural Water Management*, 82(3), 371-386. doi:10.1016/j.agwat.2005.08.001
- Allen, R. G., Pereira, L. S., Raes, D., & Smith, M. (1998). *Crop Evapotranspiration*. Rome, Italy: FAO 1998.
- Allen, R. G., Walter, I. A., Elliott, R., Howell, T., Itenfisu, D., & Jensen, M. (2005). *The ASCE standardized reference evapotranspiration equation. Final Report (ASCE-EWRI)*. ASCE Subject Headings. doi:10.1061/9780784408056
- Almorox, J., Quej, V. H., & Martí, P. (2015). Global performance ranking of temperature-based approaches for evapotranspiration estimation considering Köppen climate classes. *Journal of Hydrology*, 528, 514-522. doi:10.1016/j.jhydrol.2015.06.057
- Aschonitis, V. G., Papamichail, D., Demertzi, K., Colombani, N., Mastrocicco, M., Ghirardini, A., . . . Fano, E. A. (2017a). High-resolution global grids of revised Priestley-Taylor and Hargreaves-Samani coefficients for assessing ASCE-standardized reference crop evapotranspiration and solar radiation. *Earth System Science Data*, 9(2), 615-638. doi:10.5194/essd-9-615-2017
- Aschonitis, V., Demertzi, K., Papamichail, D., Colombani, N., & Mastrocicco, M. (2017b). Revisiting the Priestley-Taylor method for the assessment of reference crop evapotranspiration in Italy. *Italian Journal of Agrometeorology*, 20(2), 5-18.
- Ashraf, B., Yazdani, R., Mousavi-Baygi, M., & Bannayan, M. (2014). Investigation of temporal and spatial climate variability. *Theoretical and Applied Climatology*, 118, 35-46. doi:10.1007/s00704-013-1040-8
- Baier, W., & Robertson, G. W. (1965). Estimation of latent evaporation from simple weather observations. *Agro-Meteorological Section*, 45(3), 276-284. doi:10.4141/cjps65-051
- Bakundukize, C., van Camp, M., & Walraevens, K. (2011). Estimation of Groundwater Recharge in Bugesera Region (Burundi) using Soil Moisture Budget Approach. *Geologica Belgica*, 14(1), 85-102.
- Bernardo, J. M., Casella, G., George, E. I., Girón, J., Moreno, E., Peña, D., . . . Robert, C. P. (2005). An objective Bayesian approach to interval estimation. *TEST*, 14, 317-384.
- Brouwer, C., & Heibloem, M. (1986). *IRRIGATION WATER MANAGEMENT*. Rome: Food and Agriculture Organization of the United Nations.
- Camargo, A. P., Marin, F. R., Sentelhas, P. C., & Picini, A. G. (1999). Adjust of the Thornthwaite’s method to estimate the potential evapotranspiration for arid and superhumid climates, based on daily temperature amplitude. *Rev.Bras.Agrometeorol*, 7, 251-257.
- Castañeda, L., & Rao, P. (2005). Comparison of methods for estimating reference evapotranspiration in Southern California. *Journal of Environmental Hydrology*, 13, 1-10.

- Cherlet, M., Hill, J., Von Maltitz, G., Sommer, S., Reynolds, J., & Hutchinson, C. (2018). *World atlas of desertification: Rethinking land degradation and sustainable land management*. EU publications.
- Cristea, N. C. (2013). Revised Coefficients for Priestley-Taylor and Makkink-Hansen Equations for Estimating Daily Reference Evapotranspiration. *Journal of Hydrologic Engineering*, 18(10), 1289-1300. doi:10.1061/(ASCE)HE.1943-5584.0000679
- Droogers, P., & Allen, R. G. (2002). Estimating Reference Evapotranspiration Under Inaccurate Data Conditions. *Irrigation and Drainage Systems*, 16, 33 - 45. doi:10.1023/A:1015508322413
- Feng, S., Trnka, M., Hayes, M., & Zhang, Y. (2017). Why do different drought indices show distinct future drought risk outcomes in the U.S. Great Plains? *Journal of Climate*, 30, 265-278. doi:10.1175/JCLI-D-15-0590.1
- Hamon, W. (1961). Estimating Potential Evapotranspiration. *Journal of the Hydraulics Division*, 87(3), 107-120.
- Hamon, W. R. (1963). Computation of direct runoff amounts from storm rainfall. *Sci. Hydrol. Publ*, 52-62.
- Hansen, J., Ruedy, R., Sato, M., & Lo, K. (2010). Global surface temperature change. *Reviews of Geophysics*, 48(4), 1-29.
- Hargreaves, G. H., & Samani, Z. A. (1982). Estimating Potential Evapotranspiration. *Journal of the Irrigation and Drainage Division*, 108(3), 225-230.
- Hijmans, R. J., Cameron, S. E., Parra, J. L., Jones, P. G., & Jarvis, A. (2005). Very high resolution interpolated climate surfaces for global land areas. *International Journal of Climatology*, 25, 1965-1978. doi:10.1002/joc.1276
- Holdridge, L. R. (1967). *Life zone ecology*. Costa Rica: Tropical science center.
- Irmak, S. (2008). Ecological Processes | Evapotranspiration. In *Encyclopedia of Ecology* (pp. 1432-1438). University of Nebraska–Lincoln, Lincoln, NE, USA: Elsevier B.V.
- Jain, P. K., & Sinai, G. (1985). Evapotranspiration Model for Semiarid Regions. *Journal of Irrigation and Drainage Engineering*, 11(4), 369-379. doi:10.1061/(ASCE)0733-9437(1985)111:4(369)
- Kimura, R. (2020). Global detection of aridification or increasing wetness in arid. *Natural Hazards*, 2261–2276. doi:10.1007/s11069-020-04080-y
- Kottek, M., Grieser, J., Beck, C., Rudolf, B., & Rubel, F. (2006). World map of the Köppen-Geiger climate classification updated. *Meteorologische Zeitschrift*, 15(3), 259 - 263. doi:10.1127/0941-2948/2006/0130
- Luxemburg, W. M., & Coenders A., M. J. (2017). *Hydrological processes and measurments (CIE4440 - Lecture Notes)*. Delft: TU Delft.
- Makkink, G. (1957). Testing the Penman formula by means of lysimeters. *Journal of the Institution of Water Engineers*, 11(3), 277-288.
- Malmström, V. H. (2007). A New Approach To The Classification Of Climate. *Journal of Geography*, 68(6), 351-357. doi:10.1080/00221346908981131
- McCloud, D. E. (1955). Water Requirements of Field Crops in Florida as Influenced by Climate. *Proceedings Soil and Crop Science Society of Florida*, 15, 165-172.
- McVicar, T. R., Roderick, M. L., Donohue, R. J., Li, L. T., Van Niel, T. G., Thomas, A., . . . Dinpashoh, Y. (2012b). Global review and synthesis of trends in observed terrestrial near-surface wind speeds: Implications for evaporation. *Journal of Hydrology*, 416-417, 182-205.

- Muhammad, M. K., Nashwan, M. S., Shahid, S., Ismail, T. b., & Song, Y. H. (2019). Evaluation of empirical reference evapotranspiration models using compromise programming: A case study of Peninsular Malaysia. *Sustainability (Switzerland)*, *11*(16). doi:10.3390/su11164267
- Oudin, L., Hervieu, F., Michel, C., Perrin, C., Andréassian, A., Anctil, F., & Loumagne, C. (2005). Which potential evapotranspiration input for a lumped rainfall–runoff model?: Part 2—Towards a simple and efficient potential evapotranspiration model for rainfall–runoff modelling. *Journal of Hydrology*, *303*(1-4), 290-306. doi:10.1016/j.jhydrol.2004.08.026
- Papadakis, J. (1965). *Crop Ecologic Survey in Relation to Agricultural Development of Western Pakistan*.
- Peel, M. C., Finlayson, B. L., & McMahon, T. (2007). Updated world map of the Köppen-Geiger climate classification. *Hydrology and Earth System Sciences*, *11*(5), 1633 - 1644. doi:10.5194/hess-11-1633-2007
- Peel, M. C., Finlayson, B. L., & McMahon, T. (2007). Updated world map of the Köppen-Geiger climate classification. *Hydrology and Earth System Sciences*, *11*(5), 1633 - 1644. doi:10.5194/hess-11-1633-2007
- Pereira, A. R., & Pruitt, W. O. (2004). Adaptation of the Thornthwaite scheme for estimating daily reference evapotranspiration. *Agricultural Water Management*, *66*(3), 251-257. doi:10.1016/j.agwat.2003.11.003
- Programme), U. (. (1997). *World atlas of desertification* (2nd ed.). London: UNEP.
- Quej, V. H., Javier, A., Arnaldo, J. A., & Moratiel, R. (2019). Evaluation of Temperature-Based Methods for the Estimation of Reference Evapotranspiration in the Yucatán Peninsula, Mexico. *Journal of Hydrologic Engineering*, *24*(2), 05018029-1 - 05018029-10. doi:10.1061/(ASCE)HE.1943-5584.0001747
- Rezaei, M., Valipour, M., & Valipour, M. (2016). Modelling Evapotranspiration to Increase the Accuracy of the Estimations Based on the Climatic Parameters. *Water Conservation Science and Engineering*, *1*, 197-207. doi:10.1007/s41101-016-0013-z
- Sanikhani, H., Kisi, O., Maroufpoor, E., & Yaseen, Z. M. (2019). Temperature-based modeling of reference evapotranspiration using several artificial intelligence models: application of different modeling scenarios. *Theoretical and Applied Climatology*, *135*, 449-462. doi:10.1007/s00704-018-2390-z
- Sepaskhah, A. R., & Razzaghi, F. (2009). Evaluation of the adjusted Thornthwaite and Hargreaves-Samani methods for estimation of daily evapotranspiration in a semi-arid region of Iran. *Archives of Agronomy and Soil Science*, *1*, 51-66. doi:10.1080/03650340802383148
- Sheffield, J., Wood, E. F., & Roderick, M. L. (2012). Little change in global drought over the past 60 years. *Nature*, *491*, 435-438. doi:10.1038/nature11575
- Sun, X., Ren, G., Xu, W., Li, Q., & Ren, Y. (2017). Global land-surface air temperature change based on the new CMA GLSAT data set. *Science Bulletin*, *62*(4), 236-238.
- Tegos, A., Malamos, N., & Koutsoyiannis, D. (2015). A parsimonious regional parametric evapotranspiration model based on a simplification of the Penman-Monteith formula. *Journal of Hydrology*, *708*-717.
- Thornthwaite, C. (1948). An Approach toward a Rational Classification of Climate. *Geographical Review*, *38*(1), 55-94. doi:10.2307/210739

- Todorovic, M., Karic, B., & Pereira, L. S. (2013). Reference evapotranspiration estimate with limited weather data across a range of Mediterranean climates. *Journal of Hydrology*, *481*, 166-176. doi:10.1016/j.jhydrol.2012.12.034
- Trajkovic, S. (2005). Temperature-Based Approaches for Estimating Reference Evapotranspiration. *Journal of Irrigation and Drainage Engineering*, *131*(4), 316-323. doi:10.1061/(ASCE)0733-9437(2005)131:4(316)
- Trajkovic, S. (2007). Hargreaves versus Penman-Monteith under humid conditions. *Journal of Irrigation and Drainage Engineering*, *133*(1), 38-42. doi:10.1061/(ASCE)0733-9437(2007)133:1(38)
- Trajkovic, S., & Kolakovic, S. (2009a). Evaluation of reference evapotranspiration equations under humid conditions. *Water Resources Management*, *23*(3057), 3057-3067. doi:doi.org/10.1007/s11269-009-9423-4
- Trajkovic, S., & Kolakovic, S. (2009b). Estimating reference evapotranspiration using limited weather data. *Journal of Irrigation and Drainage Engineering*, *135*(4), 443-449. doi:10.1061/(ASCE)IR.1943-4774.0000094
- Trajkovic, S., Gocic, M., Pongracz, R., Bartholy, J., & Milanovic, M. (2020). Assessment of Reference Evapotranspiration by Regionally Calibrated Temperature-Based Equations. *KSCE Journal of Civil Engineering*, *24*, 1020-1027. doi:10.1007/s12205-020-1698-2
- Trenberth, K. E., Dai, A., Van Der Schrier, G., Jones, P. D., Barichivich, J., Briffa, K. R., & Sheffield, J. (2014). Global warming and changes in drought. *Nature Climate Change*, *4*, 17-22. doi:10.1038/nclimate2067
- Turc, L. (1961). Water requirements assessment of irrigation, potential evapotranspiration: Simplified and updated climatic formula. *Annales Agronomiques*, *12*, 13-49.
- UNEP. (1997). World Atlas of Desertification. In N. Middleton, Thomas, & D.. London: United Nations Environment Programme.
- Valiantzas, J. D. (2013a). Simplified forms for the standardized FAO-56 Penman–Monteith reference evapotranspiration using limited weather data. *Journal of Hydrology*, *505*, 13-23. doi:10.1016/j.jhydrol.2013.09.005
- Valiantzas, J. D. (2013b). Simple ET₀ Forms of Penman’s Equation without Wind and/or Humidity Data. I: Theoretical Development. *Journal of Irrigation and Drainage Engineering*, *139*(1), 1-8. doi:10.1061/(asce)ir.1943-4774.0000520
- Valiantzas, J. D. (2014). Closure to “Simple ET₀ Forms of Penman’s Equation without Wind and/or Humidity Data. I: Theoretical Development” by John D. Valiantzas. *Journal of Irrigation and Drainage Engineering*, *140*(7), 07014017-1. doi:10.1061/(asce)ir.1943-4774.0000750
- Valipour, M., Gholami Sefidkouhi, M. A., & Raeini–Sarjaz, M. (2017). Selecting the best model to estimate potential evapotranspiration with respect to climate change and magnitudes of extreme events. *Agricultural Water Management*, *180* (A), 50-60. doi:10.1016/j.agwat.2016.08.025
- Van Der Schrier, G., Barichivich, J., Briffa, K. R., & Jones, P. D. (2013). A scPDSI-based global data set of dry and wet spells for 1901-2009. *Journal of Geophysical Research Atmospheres*, *118*(10), 4025-4048. doi:10.1002/jgrd.50355
- Wild, M., Folini, D., Schär, C., Loeb, N., Dutton, E. G., & König-Langlo, G. (2013). The global energy balance from a surface perspective. *Climate Dynamics*, *40*(11-12), 3107-3134.
- Willett, K. M., Dunn, R. J., Thorne, P. W., Bell, S., De Podesta, M., Parker, D. E., . . . Williams, C. N. (2014). HadISDH land surface multi-variable humidity and

- temperature record for climate monitoring. *Climate of the Past*, 10(6), 1983-2006.
- Willmott, C. J., Rowe, C. M., & Mintz, Y. (1985). Climatology of the terrestrial seasonal water cycle. *Journal of Climatology*, 5(6), 589-606.
doi:10.1002/joc.3370050602
- WMO. (1966). *Measurement and estimation of evaporation and evapotranspiration: report of a working group on Evaporation measurement of the Commission for Instruments and methods of observation*. Geneva, Switzerland: WMO.
- Yang, Q., Ma, Z., Zheng, Z., & Duan, Y. (2017). Sensitivity of potential evapotranspiration estimation to the Thornthwaite and Penman–Monteith methods in the study of global drylands. *Advances in Atmospheric Sciences*, 34(12), 1381-1394. doi:10.1007/s00376-017-6313-1
- Yuan, S., & Qiring, S. M. (2014). Drought in the U.S. Great Plains (1980–2012): A sensitivity study using different methods for estimating potential evapotranspiration in the Palmer Drought Severity Index. *Journal of Geophysical Research: Atmospheres*, 119(19), 10996 - 11010.
doi:10.1002/2014JD021970
- Zhang, J., Sun, F., Xu, J., Chen, Y., Sang, Y. F., & Liu, C. (2016). Dependence of trends in and sensitivity of drought over China (1961-2013) on potential evaporation model. *Geophysical Research Letters*, 43(1), 206-213.
doi:10.1002/2015GL067473
- Zhang, Y., & Liang, C. (2020). Analysis of Annual and Seasonal Precipitation Variation in the Qinba Mountain area, China. *Scientific Reports*, 1 - 13.
- Zhang, Y., Liu, S., Wei, X., Liu, J., & Zhang, G. (2008). Potential impact of afforestation on water yield in the subalpine region of southwestern China. *Journal of the American Water Resources Association*, 44(5), 1144-1153.
doi:10.1111/j.1752-1688.2008.00239.x

Supplementary Material

Table S1:

Ground stations California Australia Europe

No.	Code	Station	Region	Altitude (m)	Lat (Dec.deg.)	Long (Dec.Deg.)	Period	Köppen Class**
CA-1	6	Davis	USA-CA	18	38.54	-121.78	Sep 1982 - Aug 2016	Csa
CA-2	2	FivePoints	USA-CA	87	36.34	-120.11	Jun 1982 - Aug 2016	BSk
CA-3	5	Shafter	USA-CA	110	35.53	-119.28	Jun 1982 - Aug 2016	BWk
CA-4	7	Firebaugh/Telles	USA-CA	56	36.85	-120.59	Sep 1982 - Aug 2016	BSk
CA-5	12	Durham	USA-CA	40	39.61	-121.82	Oct 1982 - Aug 2016	Csa
CA-6	8	Gerber	USA-CA	76	40.04	-122.17	Sep 1982 - Aug 2014	Csa
CA-7	15	Stratford	USA-CA	59	36.16	-119.85	Nov 1982 - Aug 2016	BSk
CA-8	19	Castroville	USA-CA	3	36.77	-121.77	Nov 1982 - Aug 2016	Csb
CA-9	21	Kettleman	USA-CA	104	35.87	-119.89	Nov 1982 - Aug 2016	BSh
CA-10	27	Zamora	USA-CA	15	38.81	-121.91	Dec 1982 - May 2006	Cfa
CA-11	30	Nicolaus	USA-CA	10	38.87	-121.55	Jan 1983 - Dec 2011	Csa
CA-12	32	Colusa	USA-CA	17	39.23	-122.02	Jan 1983 - Aug 2016	Csa
CA-13	33	Visalia	USA-CA	107	36.3	-119.22	Jan 1983 - Feb 2007	BSk
CA-14	35	Bishop	USA-CA	1271	37.36	-118.41	Feb 1983 - Aug 2016	BWk
CA-15	39	Parlier	USA-CA	103	36.6	-119.5	May 1983 - Aug 2016	BSk
CA-16	41	Calipatria/Mulberry	USA-CA	-34	33.04	-115.42	Jul 1983 - Aug 2016	BWh
CA-17	43	McArthur	USA-CA	1009	41.06	-121.46	Dec 1983 - Aug 2016	Csb
CA-18	44	U.C.Riverside	USA-CA	311	33.96	-117.34	Jun 1985 - Aug 2016	BSk
CA-19	47	Brentwood	USA-CA	14	37.93	-121.66	Nov 1985 - Aug 2016	Csa
CA-20	49	Oceanside	USA-CA	15	33.26	-117.32	Mar 1986 - Oct 2003	BSk
CA-21	54	Blackwells Corner	USA-CA	215	35.65	-119.96	Oct 1986 - Aug 2016	BWk
CA-22	56	Los Banos	USA-CA	29	37.1	-120.75	Jun 1988 - Aug 2016	BSk
CA-23	61	Orland	USA-CA	60	39.69	-122.15	May 1987 - May 2010	Csa
CA-24	62	Temecula	USA-CA	433	33.49	-117.23	Nov 1986 - Aug 2016	Csa
CA-25	64	Santa Ynez	USA-CA	149	34.58	-120.08	Nov 1986 - Aug 2016	Csb
CA-26	68	Seeley	USA-CA	12	32.76	-115.73	May 1987 - Aug 2016	BWh
CA-27	70	Manteca	USA-CA	10	37.83	-121.22	Nov 1987 - Aug 2016	Csa
CA-28	71	Modesto	USA-CA	11	37.65	-121.19	Jul 1987 - Aug 2016	BSk
CA-29	77	Oakville	USA-CA	58	38.43	-122.41	Jan 1989 - Aug 2016	Csb
CA-30	75	Irvine	USA-CA	125	33.69	-117.72	Oct 1987 - Aug 2016	BSk
CA-31	78	Pomona	USA-CA	223	34.06	-117.81	Mar 1989 - Aug 2016	Csa
CA-32	80	Fresno State	USA-CA	103	36.82	-119.74	Oct 1988 - Aug 2016	BSk
CA-33	83	Santa Rosa	USA-CA	24	38.4	-122.8	Jan 1990 - Aug 2016	Csb
CA-34	84	Browns Valley	USA-CA	287	39.25	-121.32	Apr 1989 - Aug 2016	Csa
CA-35	85	Hopland F.S.	USA-CA	354	39.01	-123.08	Sep 1989 - Apr 2016	Csa

CA-36	86	Lindcove	USA-CA	146	36.36	-119.06	May 1989 - Aug 2016	BSk
CA-37	87	Meloland	USA-CA	-15	32.81	-115.45	Dec 1989 - Aug 2016	BWh
CA-38	88	Cuyama	USA-CA	698	34.94	-119.67	May 1989 - Aug 2016	BWk
CA-39	91	Tulelake F.S.	USA-CA	1230	41.96	-121.47	Mar 1989 - Aug 2016	BSk
CA-40	92	Kesterson	USA-CA	23	37.23	-120.88	Oct 1989 - Aug 2016	BSk
CA-41	94	Goletta foothills	USA-CA	195	34.47	-119.87	Jul 1989 - Jul 2016	Csb
CA-42	99	Santa Monica	USA-CA	104	34.04	-118.48	Dec 1992 - Aug 2016	BSk
CA-43	103	Windsor	USA-CA	26	38.53	-122.83	Dec 1990 - Aug 2016	Csb
CA-44	104	De Laveaga	USA-CA	91	37	-122	Sep 1990 - Aug 2016	Csb
CA-45	105	Westlands	USA-CA	58	36.63	-120.38	Apr 1992 - Aug 2016	BSk
CA-46	106	Sanel Valley	USA-CA	160	38.98	-123.09	Feb 1991 - Aug 2016	Csb
CA-47	57	Buntingville	USA-CA	1221	40.29	-120.43	June 1986 - Sep 2016	Dsb
CA-48	90	Alturas	USA-CA	1343	41.44	-120.48	Apr 1989 - Sep 2016	Dsb
CA-49	151	Ripley	USA-CA	77	33.53	-114.63	Dec 1998 - Sep 2016	BWh
CA-50	183	Owens Lake North	USA-CA	1123	36.49	-117.92	Dec 2002 - Sep 2016	BWk
CA-51	147	Otay Lake	USA-CA	177	32.63	-116.94	Apr 1999 - Sep 2016	BWk
CA-52	175	Palo Verde II	USA-CA	70	33.38	-114.72	Jan 2001 - Sep 2016	BWh
CA-53	135	Blynthe NE	USA-CA	84	33.66	-114.56	Jan 1997 - Sep 2016	BWh
CA-54	155	Bryte	USA-CA	12	38.6	-121.54	Dec 1998 - Sep 2016	Csa
CA-55	159	Monrovia	USA-CA	181	34.15	-117.99	Oct 1999 - Sep 2016	Csa
CA-56	161	Patterson	USA-CA	56	37.44	-121.14	Aug 1999 - Sep 2016	BSk
CA-57	174	Long Beach	USA-CA	5	33.8	-118.09	Sep 2000 - Sep 2016	BSk
CA-58	173	Torrey Pines	USA-CA	102	32.9	-117.25	Nov 2000 - Sep 2016	BSk
CA-59	150	Miramar	USA-CA	136	32.89	-117.14	Apr 1999 - Sep 2016	BSk
CA-60	153	Escondido SPV	USA-CA	119	33.08	-116.98	Feb 1999 - Sep 2016	BSk
A-1	32040	Townsville Aero	Australia	4	-19.25	146.77	(1940/1996-2016)#	As
A-2	33307	Woolshed	Australia	556	-19.42	146.54	(1990/2003-2016)	Csa
A-3	2056	Kununurra Aero	Australia	44	-15.78	128.71	(1971/1990-2016)	BSh
A-4	35264	Emerald	Australia	189	-23.57	148.18	(1990/1998-2016)	BSh
A-5	24024	Loxton R.C.	Australia	30	-34.44	140.6	(1984/1998-2016)	BSk
A-6	74037	Yanco AGI.	Australia	164	-34.62	146.43	(1957/1999-2016)	BSk
A-7	74258	Deniliquin Airp.AWS	Australia	94	-35.56	144.95	(1990/2003-2016)	BSk
A-8	75041	Griffith Airp.AWS	Australia	134	-34.25	146.07	(1958/1990-2016)	BSk
A-9	76031	Mildura Airp.	Australia	50	-34.24	142.09	(1946/1993-2016)	BSk
A-10	24048	Renmark Apt.1	Australia	32	-34.2	140.68	(1990/2003-2016)	BWk
A-11	40082	University of QLD G.	Australia	89	-27.54	152.34	(1897/1995-2016)	Cfa
A-12	40922	Kingaroy Airp.	Australia	434	-26.57	151.84	(1990/2003-2016)	Cfa
A-13	41359	Oakey Aero	Australia	406	-27.4	151.74	(1970/1996-2016)	Cfa
A-14	41522	Dalby Airp.	Australia	344	-27.16	151.26	(1990/2006-2016)	BSh
A-15	41525	Warwick	Australia	475	-28.21	152.1	(1990/2000-2016)	Cfa
A-16	41529	Toowoomba Airp.	Australia	641	-27.54	151.91	(1990/1997-2016)	Cfa
A-17	80091	Kyabram	Australia	105	-36.34	145.06	(1964/1990-2016)	Cfa
A-18	81049	Tatura I.S.A.	Australia	114	-36.44	145.27	(1942/1990-2016)	Cfa
A-19	81124	Yarrawonga	Australia	129	-36.03	146.03	(1990/2003-2016)	Cfa

A-20	81125	Shepparton Airp.	Australia	114	-36.43	145.39	(1990/1996-2016)	BSk
A-21	41175	Applethorpe	Australia	872	-28.62	151.95	(1966/2006-2016)	Cfb
A-22	81123	Bendigo Airp.	Australia	208	-36.74	144.33	(1990/2004-2016)	Cfa
A-23	85072	East sale Airp.	Australia	5	-38.12	147.13	(1943/1996-2016)	Cfb
A-24	85279	Bairnsdale Airp.	Australia	49	-37.88	147.57	(1942/2003-2016)	Cfb
A-25	85280	Morwell L.V.Airp.	Australia	56	-38.21	146.47	(1984/1999-2016)	Cfb
A-26	85296	Mount Moomapa	Australia	480	-37.75	147.14	(1990/2003-2016)	Cfb
A-27	90035	Colac	Australia	261	-38.23	143.79	(1990/2003-2016)	Cfb
A-28	9538	Dwellingup	Australia	267	-32.71	116.06	(1934/1990-2016)	Csa
A-29	9617	Bridgetown	Australia	179	-33.95	116.13	(1990/2003-2016)	Csb
A-30	23373	Nuriootpa Pirs	Australia	275	-34.48	139.01	(1990/1996-2016)	Csa
A-31	26021	Mount Gambier Aero	Australia	63	-37.75	140.77	(1942/1994-2016)	Csb
A-32	26091	Coonawarra	Australia	57	-37.29	140.83	(1985/1990-2016)	Csb
A-33	66062	Sydney (Obs.Hill)	Australia	39	-33.86	151.205	(1858/1990-2016)	Cfa
A-34	33002	Ayr DPI Res.St.	Australia	17	-19.62	147.38	(1951/1994-2016)	As
A-35	7176	Newman Aero	Australia	524	-23.42	119.8	(1971/2003-2016)	BWh
A-36	13017	Giles	Australia	598	-25.03	128.3	(1956/1990-2016)	BWh
A-37	11052	Forrest	Australia	159	-30.85	128.11	(1990/2003-2016)	BWh
A-38	11003	Eucla	Australia	93	-31.68	128.9	(1876/1995-2016)	BSk
A-39	12071	Salmon Gums	Australia	249	-32.99	121.62	(1932/2003-2016)	BSk
A-40	7045	Meekatharra Airp.	Australia	517	-26.61	118.54	(1944/1992-2016)	BWh
A-41	1025	Doongan	Australia	385	-15.38	126.31	(1988/1990-2016)	As
A-42	2012	Halls Creek Airp.	Australia	422	-18.23	127.66	(1944/1996-2016)	BSh
A-43	13015	Carnegie	Australia	448	-25.8	122.98	(1942/1990-2016)	BWh
A-44	3080	Curtin Aero	Australia	78	-17.58	123.83	(1990/2003-2016)	BSh
A-45	6022	Gascoyne Junction	Australia	144	-25.05	115.21	(1907/1990-2016)	BWh
A-46	9789	Esperance	Australia	25	-33.83	121.89	(1969/1990-2016)	Csb
A-47	91223	Marawah	Australia	107	-40.91	144.71	(1971/1990-2016)	Cfb
A-48	18106	Nullarbor	Australia	64	-31.45	130.9	(1986/2006-2016)	BSk
A-49	16090	Cooper Pedy Airp.	Australia	225	-29.03	134.72	(1990/2004-2016)	BWh
A-50	16085	Marla Police St.	Australia	323	-27.3	133.62	(1985/1990-2016)	BWh
A-51	13011	Warburton Airfield	Australia	459	-26.13	126.58	(1940/2003-2016)	BWh
A-52	15528	Yuendumu	Australia	667	-22.26	131.8	(1952/1990-2016)	BWh
A-53	15666	Rabbit Flat	Australia	340	-20.18	130.01	(1990/1996-2016)	BSh
A-54	14829	Lajamanu Airp.	Australia	316	-18.33	130.64	(1952/1990-2016)	BSh
A-55	15135	Tennant Creek Airp.	Australia	376	-19.64	134.18	(1969/1992-2016)	BSh
A-56	37010	Camooweal Township	Australia	231	-19.92	138.12	(1891/2003-2016)	BSh
A-57	14707	Wollogorang	Australia	60	-17.21	137.95	(1967/1990-2016)	As
A-58	14938	Mango Farm	Australia	15	-13.74	130.68	(1980/1990-2016)	Aw
A-59	69134	Batemans Bay	Australia	11	-35.72	150.19	(1985/1991-2016)	Cfb
A-60	14198	Jabiru Airp.	Australia	27	-12.66	132.89	(1971/1990-2016)	Aw
A-61	28008	Lockhart River Airp.	Australia	19	-12.79	143.3	(1956/2001-2016)	Aw
A-62	34084	Charters Towers Airp.	Australia	290	-20.05	146.27	(1990/1992-2016)	BSh
A-63	29038	Kowanyama Airp.	Australia	10	-15.48	141.75	(1912/1999-2016)	As
A-64	32078	Ingham Composite	Australia	12	-18.65	146.18	(1968/1990-2016)	Am
A-65	40854	Logan City W.T.P.	Australia	14	-27.68	153.19	(1990/1992-2016)	Cfa
A-66	8095	Mullewa	Australia	268	-28.54	115.51	(1896/1990-2016)	BSh
A-67	8251	Kalbarri	Australia	6	-27.71	114.17	(1970/1990-2016)	BSh
A-68	8225	Eneabba	Australia	100	-29.82	115.27	(1964/1990-2016)	Csa
A-69	7139	Paynes find	Australia	339	-28.5	119.74	(1919/1990-2016)	BSh
A-70	10007	Bencubbin	Australia	359	-30.81	117.86	(1912/1990-2016)	BSh
A-71	10092	Merredin	Australia	315	-31.48	118.28	(1903/1990-2016)	BSh
A-72	12038	Kalgoorlie-Boulder Airp.	Australia	365	-30.78	121.45	(1939/1994-2016)	BSh
A-73	16098	Tarcoola Aero	Australia	123	-30.71	134.58	(1990/1999-2016)	BWh
A-74	18195	Minnipa Pirs	Australia	165	-32.84	135.15	(1990/2003-2016)	BSk
A-75	46126	Tibooburra Airp.	Australia	176	-29.44	142.06	(1990/2003-2016)	BWh
A-76	48245	Boorke Airp. AWS	Australia	107	-30.04	145.95	(1990/2002-2016)	BSh

A-77	55325	Tamworth Airp. AWS	Australia	395	-31.07	150.84	(1990/2006-2016)	Cfa
A-78	38026	Birdsville Airp.	Australia	47	-25.9	139.35	(1990/2001-2016)	BWh
A-79	30161	Richmond Airp.	Australia	206	-20.7	143.12	(1990/2003-2016)	BSh
A-80	33013	Collinsville Airp.	Australia	196	-20.55	147.85	(1939/1990-2016)	BSh
Eu-1	32	Bourges	Europe	161	47.059	2.359	Mar 1987 - Jul 2020	Cfb
Eu-2	34	Bordeaux-Merignac	Europe	47	44.831	-0.691	Jan 1978 - May 2020	Cfb
Eu-3	36	Perpignan	Europe	42	42.737	2.873	Jan 1931 - Aug 2020	Csa
Eu-4	39	Marignane	Europe	9	43.438	5.216	Dec 1960 - Jun 2020	Csa
Eu-5	40	Bamberg	Europe	240	49.875	10.922	Oct 1954 - Sep 2020	Dfb
Eu-6	42	Bremen	Europe	4	53.046	8.799	Jan 1936 - Sep 2020	Cfb
Eu-7	43	Dresden Wahnisdorf	Europe	246	51.117	13.683	Jan 1934 - Sep 2020	Dfb
Eu-8	44	Frankfurt	Europe	112	50.046	8.598	Jul 1935 - Sep 2020	Cfb
Eu-9	45	Halle	Europe	93	51.514	11.951	Dec 1953 - Mar 2015	Cfb
Eu-10	47	Hamburg Fuhlsbuettel	Europe	11	53.635	9.99	Sep 1938 - Sep 2020	Cfb
Eu-11	48	Hohenpeissenberg	Europe	977	47.802	11.012	Jan 1937 - Sep 2020	Dfb
Eu-12	51	Karlsruhe	Europe	112	49.039	8.365	Jan 1936 - Sep 2020	Cfb
Eu-13	52	Muenchen	Europe	515	48.164	11.544	Jan 1936 - Sep 2020	Dfb
Eu-14	54	Potsdam	Europe	81	52.383	13.064	1/01/1893 - Sep 2020	Dfb
Eu-15	58	Zugspitze	Europe	2964	47.422	10.987	Aug 1900 - Sep 2020	ET
Eu-16	66	Reykjavik	Europe	52	64.127	-21.903	Jan 1964 - Sep 2020	Dfc
Eu-17	120	Birr	Europe	70	53.09	-7.876	Oct 1954 - Dec 2017	Cfb
Eu-18	121	Dublin Phoenix Park	Europe	49	53.364	-6.319	01/09/1895 - Sep 2020	Cfb
Eu-19	122	Malin Head	Europe	21	55.372	-7.34	Jun 1981 - Oct 2018	Cfb
Eu-20	123	Valentia Observatory	Europe	9	51.939	-10.222	Oct 1939 - Oct 2018	Cfb
Eu-21	161	De Kooy	Europe	1	52.927	4.781	Sep 1908 - Sep 2020	Cfb
Eu-22	162	De Bilt	Europe	1	52.099	5.179	Jan 1901 - Sep 2020	Cfb
Eu-23	164	Eelde	Europe	5	53.123	6.584	Jan 1906 - Sep 2020	Cfb
Eu-24	166	Vlissingen	Europe	8	51.441	3.596	Jan 1907 - Sep 2020	Cfb
Eu-25	168	Maastricht	Europe	114	50.905	5.762	Jan 1906 - Sep 2020	Cfb
Eu-26	190	Karasjok	Europe	129	69.467	25.503	Jan 1961 - Nov 2020	Dfc
Eu-27	193	Oslo Blindern	Europe	94	59.943	10.721	Jan 1952 - Dec 2020	Dfb
Eu-28	227	Hurbanovo	Europe	115	47.867	18.183	Jan 1951 - Apr 2020	Dfb
Eu-29	228	Ljubljana Bezigrad	Europe	299	46.066	14.513	Jan 1948 - Sep 2020	Dfb
Eu-30	229	Badajoz/Talavera La Real	Europe	185	38.883	-6.829	Apr 1955 - Sep 2020	Csa
Eu-31	230	Madrid - Retiro	Europe	667	40.412	-3.678	Jan 1920 - Sep 2020	BSk
Eu-32	231	Malaga Aeropuerto	Europe	7	36.667	-4.488	Dec 1947 - Sep 2020	Csa
Eu-33	232	Navacerrada	Europe	1894	40.781	-4.01	Mar 1951 - Sep 2020	Dsb
Eu-34	233	Salamanca Aeropuerto	Europe	790	40.959	-5.498	Jan 1951 - Sep 2020	BSk
Eu-35	234	San Sebastian - Igueldo	Europe	251	43.308	-2.039	Jan 1933 - Sep 2020	Cfb

Eu-36	237	Valencia	Europe	11	39.481	-0.366	Feb 1938 - Sep 2020	BSk
Eu-37	238	Zaragoza Aeropuerto	Europe	247	41.662	-1.008	Jan 1951 - Sep 2020	BSk
Eu-38	265	Bergen Florida	Europe	12	60.383	5.333	Jan 1957 - Sep 2020	Cfb
Eu-39	266	Bodoe Vi	Europe	11	67.267	14.359	Jan 1961 - Sep 2020	Dfc
Eu-40	268	Voru	Europe	82	57.846	27.019	Jan 1966 - Dec 2020	Dfb
Eu-41	309	Alicante El Altet	Europe	43	38.283	-0.571	Mar 1967 - Sep 2020	BSH
Eu-42	322	Rennes-St Jacques	Europe	36	48.069	-1.734	Oct 1967 - Aug 2020	Cfb
Eu-43	323	Strasbourg-Entzheim	Europe	150	48.549	7.64	Aug 1974 - Jul 2020	Cfb
Eu-44	324	Lindenberg	Europe	98	52.209	14.12	Jun 1906 - Sep 2020	Dfb
Eu-45	328	Tromso	Europe	100	69.654	18.928	Jan 1961 - Nov 2020	Dfc
Eu-46	334	Poprad/Tatry	Europe	694	49.067	20.233	Jan 1951 - Apr 2020	Dfb
Eu-47	336	Albacete Los Llanos	Europe	704	38.952	-1.863	Jan 1951 - Sep 2020	BSk
Eu-48	337	Cordoba Aeropuerto	Europe	90	37.844	-4.846	Apr 1959 - Sep 2020	Csa
Eu-49	356	Aachen	Europe	202	50.784	6.095	Jan 1935 - Apr 2011	Cfb
Eu-50	411	Marknesse	Europe	-3	52.702	5.887	Sep 1993 - Sep 2020	Cfb
Eu-51	412	Alicante	Europe	81	38.373	-0.494	Sep 1938 - Sep 2020	BSH
Eu-52	413	Lauwersoog	Europe	2	53.412	6.199	Mar 1991 - Sep 2020	Cfb
Eu-53	414	Burgos-Villafria	Europe	890	42.356	-3.633	Jan 1951 - Sep 2020	Cfb
Eu-54	415	Cadiz	Europe	1	36.501	-6.257	Oct 1955 - Dec 2017	Csa
Eu-55	416	Ciudad Real	Europe	628	38.989	-3.919	Jan 1951 - Sep 2020	BSk
Eu-56	417	Granada	Europe	687	37.137	-3.631	Jun 1941 - Sep 2020	Csa
Eu-57	418	Huelva (Ronda Del Este)	Europe	19	37.28	-6.909	Jul 1951 - Sep 2020	Csa
Eu-58	419	Huesca	Europe	541	42.083	-0.326	Jan 1951 - Sep 2020	Cfa
Eu-59	420	A Coruna	Europe	58	43.367	-8.419	Jan 1951 - Sep 2020	Csb
Eu-60	421	Murcia	Europe	61	38.003	-1.169	Jan 1961 - Sep 2020	BSH
Eu-61	422	Pamplona	Europe	459	42.777	-1.65	Oct 1953 - Sep 2020	Cfb
Eu-62	423	Sevilla/San Pablo	Europe	34	37.417	-5.879	Jan 1951 - Sep 2020	Csa
Eu-63	424	Soria	Europe	1082	41.775	-2.483	Jan 1951 - Sep 2020	Cfb
Eu-64	425	Valladolid	Europe	735	41.65	-4.767	Oct 1973 - Sep 2020	Csa
Eu-65	434	Brest-Guipavas	Europe	94	48.444	-4.412	Mar 1987 - Jul 2020	Cfb
Eu-66	438	Cabauw	Europe	0	51.969	4.926	Aug 1986 - Sep 2020	Cfb
Eu-67	442	Volkel	Europe	20	51.658	5.707	Oct 1992 - Sep 2020	Cfb
Eu-68	451	Berkhout	Europe	-2	52.643	4.979	Mar 1999 - Sep 2020	Cfb
Eu-69	453	Heino	Europe	3	52.434	6.259	Jul 1993 - Sep 2020	Cfb
Eu-70	454	Hupsel	Europe	29	52.068	6.657	Oct 1989 - Sep 2020	Cfb
Eu-71	455	Tenerife/Los Rodeos	Europe	632	28.478	-16.329	Aug 1941 - Sep 2020	Csb
Eu-72	462	Goteborg A	Europe	5	57.716	11.994	Jan 1983 - Sep 2020	Dfb

Eu-73	464	Arcen	Europe	19	51.497	6.196	Feb 1991 - Sep 2020	Cfb
Eu-74	469	List/Sylt	Europe	26	55.013	8.413	Aug 1972 - Sep 2020	Cfb
Eu-75	470	Schleswig	Europe	43	54.529	9.549	May 1949 - Sep 2020	Cfb
Eu-76	471	Westermarkelsdorf/Fehmarn	Europe	3	54.529	11.062	Mar 1950 - Sep 2020	Cfb
Eu-77	472	Rostock-Warnemunde	Europe	4	54.182	12.082	Jan 1951 - Sep 2020	Cfb
Eu-78	473	Greifswald	Europe	2	54.098	13.408	Feb 1936 - Sep 2020	Dfb
Eu-79	474	Emden-Flugplatz	Europe	0	53.389	7.227	Aug 1947 - Sep 2020	Cfb
Eu-80	475	Neuruppin	Europe	38	52.905	12.808	Jan 1962 - Apr 2019	Dfb
Eu-81	476	Hannover	Europe	55	52.466	9.679	Jan 1936 - Sep 2020	Cfb
Eu-82	477	Magdeburg	Europe	76	52.103	11.584	Oct 1934 - Sep 2020	Cfb
Eu-83	478	Herwijnen	Europe	0	51.858	5.145	Mar 1990 - Sep 2020	Cfb
Eu-84	479	Dusseldorf	Europe	37	51.297	6.77	Jan 1935 - Sep 2020	Cfb
Eu-85	480	Kassel	Europe	231	51.298	9.443	Jan 1951 - Nov 2013	Cfb
Eu-86	482	Leipzig-Schkeuditz	Europe	131	51.436	12.241	Jan 1934 - Sep 2020	Cfb
Eu-87	483	Dresden-Klotzsche	Europe	227	51.129	13.756	Jan 1934 - Sep 2020	Dfb
Eu-88	484	Gorlitz	Europe	238	51.163	14.953	Jan 1951 - Sep 2020	Dfb
Eu-89	485	Nurburg-Barweiler	Europe	485	50.361	6.87	Mar 1995 - Sep 2020	Cfb
Eu-90	486	Meiningen	Europe	450	50.563	10.377	Jan 1979 - Sep 2020	Dfb
Eu-91	487	Erfurt-Bindersleben	Europe	316	50.984	10.963	Jan 1951 - Sep 2020	Dfb
Eu-92	488	Fichtelberg	Europe	1213	50.429	12.955	Oct 1921 - Sep 2020	Dfc
Eu-93	489	Wurzburg	Europe	268	49.771	9.959	Jan 1947 - Sep 2020	Cfb
Eu-94	490	Hof	Europe	565	50.313	11.878	Jan 1947 - Sep 2020	Dfb
Eu-95	491	Saarbrücken/Ensheim	Europe	320	49.214	7.108	Sep 1955 - Sep 2020	Cfb
Eu-96	492	Nurnberg	Europe	314	49.504	11.057	Jan 1936 - Sep 2020	Dfb
Eu-97	493	Straubing	Europe	351	48.828	12.56	Jan 1951 - Sep 2020	Dfb
Eu-98	494	Augsburg	Europe	461	48.426	10.943	Jan 1947 - Sep 2020	Dfb
Eu-99	495	Konstanz	Europe	443	47.678	9.191	Jan 1946 - Sep 2020	Cfb
Eu-100	496	Kempten	Europe	705	47.724	10.336	Jan 1952 - Sep 2020	Dfb
Eu-101	500	Nieuw Beerta	Europe	0	53.194	7.149	Jan 1990 - Sep 2020	Cfb
Eu-102	567	Wilhelminadorp	Europe	1	51.526	3.883	Nov 1989 - Sep 2020	Cfb
Eu-103	593	Schiphol	Europe	-3	52.316	4.79	Jan 1963 - Sep 2020	Cfb
Eu-104	594	Hoorn Terschelling	Europe	0	53.391	5.346	Jun 1994 - Sep 2020	Cfb
Eu-105	596	Stavoren	Europe	-1	52.897	5.383	Aug 1993 - Sep 2020	Cfb
Eu-106	597	Lelystad	Europe	-3	52.457	5.519	Jan 1990 - Sep 2020	Cfb
Eu-107	598	Rotterdam	Europe	-4	51.961	4.447	Jan 1978 - Sep 2020	Cfb
Eu-108	599	Gilze-Rijen	Europe	11	51.565	4.935	Nov 1951 - Sep 2020	Cfb
Eu-109	600	Ell	Europe	30	51.197	5.763	Jul 1999 - Sep 2020	Cfb

Eu-110	602	Hoek Van Holland	Europe	11	51.991	4.122	Aug 1995 - Sep 2020	Cfb
Eu-111	603	Leeuwarden	Europe	0	53.223	5.752	Sep 1955 - Sep 2020	Cfb
Eu-112	738	Caen-Carpiquet	Europe	67	49.18	-0.456	Jan 1974 - May 2020	Cfb
Eu-113	742	Nantes-Bouguenais	Europe	26	47.15	-1.609	Mar 1986 - Jul 2020	Cfb
Eu-114	745	Dijon-Longvic	Europe	219	47.268	5.088	Oct 1976 - Jul 2020	Cfb
Eu-115	750	Clermont-Ferrand	Europe	331	45.787	3.149	Jan 1978 - Aug 2020	Cfb
Eu-116	755	Embrun	Europe	871	44.566	6.502	Jan 1980 - Aug 2020	Cfb
Eu-117	757	Nice	Europe	2	43.649	7.209	Oct 1967 - Dec 2017	Csa
Eu-118	758	Bastia	Europe	10	42.541	9.485	Jan 1991 - May 2020	Csa
Eu-119	786	Montelimar	Europe	73	44.581	4.733	Jan 1949 - May 2020	Cfa
Eu-120	812	Kahler Asten (Wst)	Europe	839	51.182	8.49	Jan 1947 - Sep 2020	Dfb
Eu-121	942	Karasjok-Markannjarga	Europe	131	69.463	25.502	Jan 1961 - Nov 2020	Dfc
Eu-122	970	Casement Aerodrome	Europe	94	53.306	-6.439	Jan 1961 - Sep 2020	Cfb
Eu-123	1042	Lyngor Fyr	Europe	4	58.633	9.15	Jan 1973 - Sep 2020	Dfb
Eu-124	1046	Sola	Europe	7	58.884	5.637	Jan 1953 - Sep 2020	Cfb
Eu-125	1052	Vaernes	Europe	12	63.5	10.89	Jan 1982 - Sep 2020	Dfb
Eu-126	1388	Izana	Europe	2371	28.309	-16.499	Jan 1920 - Sep 2020	Csb
Eu-127	1389	Melilla	Europe	47	35.278	-2.955	Sep 1970 - Sep 2020	BSH
Eu-128	1392	Santander Centro	Europe	64	43.464	-3.819	Jan 1931 - Sep 2020	Cfb
Eu-129	1393	Bilbao Aeropuerto	Europe	42	43.298	-2.906	Nov 1952 - Sep 2020	Cfb
Eu-130	1394	Santiago De Compostela/Labacolla	Europe	370	42.888	-8.411	Feb 1956 - Sep 2020	Csb
Eu-131	1395	Vigo Peinador	Europe	261	42.239	-8.624	Feb 1977 - Sep 2020	Csb
Eu-132	1396	Ponferrada	Europe	534	42.564	-6.6	Jan 1951 - Sep 2020	Csb
Eu-133	1397	Leon Virgen Del Camino	Europe	916	42.589	-5.649	Jan 1951 - Sep 2020	Csb
Eu-134	1398	Logrono-Agoncillo	Europe	353	42.452	-2.331	Oct 1951 - Sep 2020	BSK
Eu-135	1399	Zamora	Europe	656	41.517	-5.733	Jan 1951 - Sep 2020	BSK
Eu-136	1401	Reus/Aeropuerto	Europe	71	41.149	1.179	May 1953 - Sep 2020	Csa
Eu-137	1404	Murcia/San Javier	Europe	4	37.789	-0.803	Jan 1951 - Sep 2020	BSK
Eu-138	1405	Jerez De La Frontera	Europe	27	36.751	-6.056	Aug 1960 - Sep 2020	Csa
Eu-139	1718	Dublin Airport	Europe	71	53.428	-6.241	1/09/1895 - Sep 2020	Cfb
Eu-140	1752	Kredarica	Europe	2513	46.378	13.849	Jan 1955 - Sep 2020	ET
Eu-141	2006	Brocken	Europe	1142	51.8	10.62	Jan 1938 - Sep 2020	Dfc
Eu-142	2135	Roches Point	Europe	43	51.793	-8.244	Dec 1955 - Mar 2004	Cfb
Eu-143	2138	Kilkenny	Europe	63	52.67	-7.27	Jun 1957 - Oct 2009	Cfb
Eu-144	2139	Shannon	Europe	6	52.69	-8.918	Sep 1945 - Sep 2020	Cfb
Eu-145	2140	Claremorris	Europe	69	53.72	-8.98	Jan 1950 - Jun 2001	Cfb
Eu-146	2142	Clones	Europe	87	54.18	-7.23	Jan 1951 - Sep 2017	Cfb

Eu-147	2143	Belmullet	Europe	9	54.23	-10	Sep 1956 - Oct 2018	Cfb
Eu-148	2190	Tours	Europe	108	47.444	0.727	Jan 1961 - Aug 2020	Cfb
Eu-149	2195	Limoges - Bellegarde	Europe	402	45.861	1.175	Oct 1967 - Jul 2020	Cfb
Eu-150	2200	Millau	Europe	712	44.118	3.018	Oct 1967 - May 2020	Cfb
Eu-151	2209	Ajaccio	Europe	5	41.918	8.793	Jul 1970 - Apr 2020	Csa
Eu-152	2230	Bergen/Flesland	Europe	48	60.289	5.226	Apr 1965 - Dec 2020	Cfb
Eu-153	2563	Deelen	Europe	50	52.055	5.872	Jan 1963 - Sep 2020	Cfb
Eu-154	2565	Hoogeveen	Europe	15	52.749	6.573	Oct 1989 - Sep 2020	Cfb
Eu-155	2566	Eindhoven	Europe	22	51.449	5.377	Jan 1978 - Sep 2020	Cfb
Eu-156	2569	Twenthe	Europe	33	52.273	6.891	Jan 1971 - Sep 2020	Cfb
Eu-157	2570	Valkenburg	Europe	0	52.17	4.429	Sep 1951 - Sep 2020	Cfb
Eu-158	2571	Westdorpe	Europe	1	51.224	3.861	Jun 1991 - Sep 2020	Cfb
Eu-159	2605	Kise Pa Hedmark	Europe	128	60.781	10.812	Jan 1959 - Dec 2020	Dfb
Eu-160	2620	Ostre Toten - Apelsvoll	Europe	264	60.7	10.867	Mar 1987 - Dec 2020	Dfc
Eu-161	2656	Kjevik	Europe	12	58.2	8.068	Jan 1954 - Dec 2020	Dfb
Eu-162	2720	Trondheim - Voll	Europe	127	63.411	10.453	Jan 1952 - Sep 2020	Dfc
Eu-163	2733	Bodoe - Vagones	Europe	33	67.283	14.467	Jan 1961 - Sep 2020	Dfc
Eu-164	2758	Muenster/Osnabrueck (Airport)	Europe	48	52.135	7.7	Oct 1989 - Sep 2020	Cfb
Eu-165	2759	Berlin-Tempelhof	Europe	48	52.468	13.404	Feb 1936 - Sep 2020	Dfb
Eu-166	2760	Trier-Petrisberg	Europe	265	49.749	6.659	Jan 1948 - Sep 2020	Cfb
Eu-167	2762	Rheinstetten	Europe	116	48.973	8.331	Jan 1936 - Sep 2020	Cfb
Eu-168	2763	Stuttgart/Echterdingen	Europe	371	48.689	9.225	Nov 1989 - Sep 2020	Cfb
Eu-169	2764	Muenchen-Flughafen	Europe	444	48.358	11.809	Apr 1970 - Sep 2020	Dfb
Eu-170	2943	Akureyri	Europe	23	65.686	-18.1	Jan 1949 - Sep 2020	Dsc
Eu-171	2969	Barcelona/Aeropuerto	Europe	4	41.293	2.07	Jan 1951 - Sep 2020	Csa
Eu-172	2970	Lanzarote/Aeropuerto	Europe	14	28.952	-13.6	Nov 1972 - Sep 2020	BWh
Eu-173	3312	Lesce	Europe	503	46.361	14.162	Nov 1990 - Aug 2020	Dfb
Eu-174	3317	Vojsko	Europe	1065	46.025	13.902	Oct 1963 - Aug 2020	Dfb
Eu-175	3323	Postojna	Europe	533	45.766	14.193	Jan 1962 - Aug 2020	Dfb
Eu-176	3326	Bilje	Europe	55	45.896	13.624	Nov 1991 - Sep 2020	Cfa
Eu-177	3328	Novo Mesto	Europe	220	45.802	15.177	Jan 1973 - Sep 2020	Cfb
Eu-178	3329	Smartno Pri Slovenj Gradcu	Europe	444	46.489	15.111	Sep 1964 - Sep 2020	Dfb
Eu-179	3330	Letalisce Jozeta Pucnika Ljubljana	Europe	362	46.211	14.478	Apr 1964 - Aug 2020	Dfb
Eu-180	3331	Letalisce Edvarda Rusjana Maribor	Europe	264	46.479	15.682	Jun 1997 - Sep 2020	Dfb
Eu-181	3332	Portoroz-Letalisce	Europe	2	45.475	13.616	May 1974 - Sep 2020	Cfa
Eu-182	3334	Lisca	Europe	947	46.068	15.285	Jan 1985 - Sep 2020	Dfb
Eu-183	3335	Murska Sobota-Rakican	Europe	187	46.652	16.191	Jan 1961 - Sep 2020	Dfb

Eu-184	3336	Ratece-Planica	Europe	864	46.5	13.7	Jun 1972 - Aug 2020	Dfb
Eu-185	3506	Stuttgart-Schnarrenberg	Europe	314	48.829	9.201	Jul 1977 - Sep 2020	Cfb
Eu-186	3542	Kosice	Europe	230	48.667	21.217	Jan 1951 - Apr 2020	Dfb
Eu-187	3548	Gurteen	Europe	76	53.03	-8.01	Oct 1954 - Dec 2017	Cfb
Eu-188	3838	Rota	Europe	21	36.639	-6.332	Oct 1988 - Sep 2020	Csa
Eu-189	3839	Madrid/Torrejon	Europe	611	40.483	-3.45	Jan 1951 - Sep 2020	BSk
Eu-190	3903	A Coruna/Alvedro	Europe	98	43.307	-8.372	Dec 1971 - Sep 2020	Csb
Eu-191	3904	Vitoria Aerodromo	Europe	521	42.851	-2.654	Mar 1952 - Sep 2020	Cfb
Eu-192	3905	Vitoria/Foronda	Europe	513	42.872	-2.733	Mar 1952 - Sep 2020	Cfb
Eu-193	3906	Albacete Obs.	Europe	674	39.007	-1.861	Jan 1983 - Sep 2020	BSk
Eu-194	3907	Almeria	Europe	7	36.833	-2.454	Jan 1945 - Sep 2020	BSh
Eu-195	3908	Almeria/Aeropuerto	Europe	21	36.846	-2.357	Jan 1945 - Sep 2020	BSh
Eu-196	3909	Asturias/Aviles	Europe	127	43.567	-6.044	Aug 1968 - Sep 2020	Cfb
Eu-197	3910	Gijon	Europe	3	43.538	-5.642	Oct 1938 - Sep 2020	Csb
Eu-198	3911	Gijon La Merced	Europe	22	43.538	-5.642	Oct 1938 - Sep 2020	Csb
Eu-199	3912	Gijon Musel	Europe	5	43.561	-5.698	Oct 1938 - Sep 2020	Csb
Eu-200	3913	Oviedo	Europe	336	43.354	-5.873	Nov 1972 - Sep 2020	Cfb
Eu-201	3914	Avila	Europe	1130	40.659	-4.68	Feb 1953 - Sep 2020	Csb
Eu-202	3915	Avila- Ayuntamiento	Europe	1143	40.656	-4.699	Feb 1953 - Sep 2020	Csb
Eu-203	3916	Ibiza/Escodola	Europe	6	38.876	1.384	Mar 1952 - Sep 2020	BSh
Eu-204	3917	Menorca/Mao	Europe	91	39.854	4.216	Jan 1965 - Sep 2020	Csa
Eu-205	3918	Palma De Mallorca Cmt	Europe	3	39.556	2.626	Aug 1972 - Sep 2020	BSk
Eu-206	3919	Palma De Mallorca / Son San Juan	Europe	8	39.561	2.737	Aug 1972 - Sep 2020	BSk
Eu-207	3921	Caceres Ciudad	Europe	459	39.483	-6.367	Jan 1983 - Sep 2020	Csa
Eu-208	3922	Santander Cmt	Europe	52	43.492	-3.799	Jan 1931 - Sep 2020	Cfb
Eu-209	3923	Santander/Parayas	Europe	5	43.429	-3.831	Jan 1972 - Sep 2020	Cfb
Eu-210	3924	Castellon	Europe	35	39.95	-0.071	Jul 1943 - Sep 2020	BSk
Eu-211	3928	Ciudad Real (Instituto)	Europe	627	38.989	-3.928	Jan 1951 - Sep 2020	BSk
Eu-212	3929	Cuenca	Europe	945	40.067	-2.138	Jan 1951 - Sep 2020	Csa
Eu-213	3931	Girona/Costa Brava	Europe	143	41.912	2.763	Jan 1973 - Sep 2020	Cfa
Eu-214	3932	Granada/Aeropuerto	Europe	567	37.189	-3.789	Nov 1972 - Sep 2020	Csa
Eu-215	3935	Molina De Aragon	Europe	1056	40.844	-1.885	Sep 1949 - Sep 2020	Cfb
Eu-216	3937	Huelva	Europe	17	37.259	-6.949	Jul 1951 - Sep 2020	Csa
Eu-217	3938	Jaen	Europe	582	37.778	-3.807	Sep 1983 - Sep 2020	BSk
Eu-218	3940	Fuerteventura/Aeropuerto	Europe	25	28.444	-13.863	Oct 1969 - Sep 2020	BWh
Eu-219	3942	Lleida	Europe	192	41.626	0.595	Sep 1947 - Sep 2020	BSk
Eu-220	3944	Lugo/Rozas	Europe	445	43.115	-7.456	May 1985 - Sep 2020	Csb

Eu-221	3945	Colmenar Viejo/Famet	Europe	1004	40.698	-3.764	Jan 1990 - Sep 2020	Csa
Eu-222	3946	Madrid/Barajas	Europe	609	40.467	-3.556	Jan 1951 - Sep 2020	BSk
Eu-223	3947	Madrid/Cuatrovientos	Europe	687	40.378	-3.789	Jan 1920 - Sep 2020	Csa
Eu-224	3948	Madrid/Getafe	Europe	617	40.3	-3.723	Jan 1951 - Sep 2020	BSk
Eu-225	3949	Murcia/Alcantarilla	Europe	85	37.958	-1.229	Jan 1961 - Sep 2020	BSk
Eu-226	3950	Pamplona (Observatorio)	Europe	442	42.818	-1.636	Oct 1953 - Sep 2020	Cfb
Eu-227	3951	Ourense	Europe	143	42.328	-7.86	Jan 1954 - Sep 2020	Csa
Eu-228	3954	Pontevedra	Europe	108	42.44	-8.616	Oct 1985 - Sep 2020	Cfb
Eu-229	3958	La Palma/Aeropuerto	Europe	33	28.633	-17.755	Apr 1970 - Sep 2020	BSh
Eu-230	3959	Sta. Cruz De Tenerife	Europe	35	28.463	-16.255	Jan 1931 - Sep 2020	BSh
Eu-231	3960	Tenerife/Sur	Europe	64	28.048	-16.561	Sep 1980 - Sep 2020	BWh
Eu-232	3961	Segovia	Europe	1005	40.948	-4.127	Jan 1951 - Sep 2020	Cfb
Eu-233	3962	Segovia (Mariano Quintanilla)	Europe	990	40.948	-4.115	Jan 1951 - Sep 2020	Cfb
Eu-234	3963	Moron De La Frontera	Europe	87	37.158	-5.616	Jan 1956 - Sep 2020	Csa
Eu-235	3964	Calamocha	Europe	890	40.926	-1.293	Aug 1992 - Sep 2020	Cfb
Eu-236	3966	Teruel	Europe	900	40.349	-1.117	Apr 1986 - Sep 2020	BSk
Eu-237	3967	Toledo	Europe	515	39.884	-4.049	Feb 1982 - Sep 2020	BSk
Eu-238	3969	Valencia/Aeropuerto	Europe	69	39.487	-0.473	Jan 1966 - Sep 2020	BSk
Eu-239	3970	Valladolid (Villanubla)	Europe	846	41.7	-4.85	Jan 1951 - Sep 2020	Csb
Eu-240	3971	Daroca	Europe	779	41.114	-1.411	Feb 1967 - Sep 2020	Cfa
Eu-241	3987	Feldberg/Schwarzwald	Europe	1490	47.876	8.004	Jan 1945 - Sep 2020	Dfc
Eu-242	3988	Freudenstadt	Europe	797	48.454	8.41	Jan 1951 - Sep 2020	Dfb
Eu-243	3990	Gera-Leumnitz	Europe	311	50.882	12.13	May 1952 - Sep 2020	Dfb
Eu-244	3991	Giessen/Wettenberg	Europe	203	50.601	8.651	Jan 1939 - Sep 2020	Cfb
Eu-245	3992	Angermunde	Europe	54	53.033	13.993	Jan 1951 - Sep 2020	Dfb
Eu-246	3993	Grosser Arber	Europe	1436	49.114	13.135	Nov 1982 - Sep 2020	Dfc
Eu-247	3994	Arkona	Europe	42	54.682	13.437	Jan 1951 - Sep 2020	Cfb
Eu-248	3995	Kiel-Holtenau	Europe	27	54.376	10.144	Jan 1940 - Jun 2019	Cfb
Eu-249	3996	Koln-Bonn	Europe	92	50.866	7.158	Oct 1957 - Sep 2020	Cfb
Eu-250	3997	Lahr	Europe	155	48.366	7.829	Mar 1982 - Sep 2020	Cfb
Eu-251	3999	Bad Lippspringe	Europe	157	51.787	8.839	Jan 1951 - Sep 2020	Cfb
Eu-252	4000	Marnitz	Europe	81	53.324	11.933	Jan 1936 - Sep 2020	Dfb
Eu-253	4001	Norderney	Europe	11	53.714	7.153	Nov 1966 - Sep 2020	Cfb
Eu-254	4002	Oberstdorf	Europe	806	47.399	10.277	Jan 1936 - Sep 2020	Dfb
Eu-255	4003	Ohringen	Europe	276	49.208	9.518	Feb 1950 - Sep 2020	Cfb
Eu-256	4004	Regensburg	Europe	365	49.043	12.103	Dec 1947 - Sep 2020	Dfb
Eu-257	4005	Berlin-Tegel	Europe	36	52.566	13.311	Sep 1937 - Sep 2020	Dfb

Eu-258	4006	Stotten	Europe	734	48.667	9.866	Jan 1947 - Sep 2020	Dfb
Eu-259	4007	Wasserkuppe	Europe	921	50.498	9.944	Jan 1936 - Sep 2020	Dfb
Eu-260	4008	Weiden	Europe	440	49.667	12.186	Oct 1948 - Sep 2020	Dfb
Eu-261	4009	Wendelstein	Europe	1832	47.704	12.013	Jan 1951 - Sep 2012	ET
Eu-262	4010	Furstenzell	Europe	476	48.546	13.354	Mar 1997 - Sep 2020	Dfb
Eu-263	4011	Hahn	Europe	497	49.948	7.264	Nov 1998 - Sep 2020	Cfb
Eu-264	4012	Mannheim	Europe	96	49.51	8.555	Oct 1947 - Sep 2020	Cfb
Eu-265	4013	Offenbach-Wetterpark	Europe	119	50.089	8.786	Jul 1935 - Sep 2020	Cfb
Eu-266	4014	Cottbus	Europe	69	51.777	14.318	Apr 1937 - Sep 2020	Dfb
Eu-267	4015	Cuxhaven	Europe	5	53.873	8.707	Jun 1946 - Sep 2020	Cfb
Eu-268	4018	Doberlug-Kirchhain	Europe	97	51.647	13.577	Jan 1951 - Sep 2020	Dfb
Eu-269	4053	Emden-Nesserland	Europe	5	53.346	7.192	Aug 1947 - Sep 2020	Cfb
Eu-270	4054	Emden-Wolthusen	Europe	0	53.372	7.224	Aug 1947 - Sep 2020	Cfb
Eu-271	4074	Essen-Bredeneu	Europe	150	51.406	6.968	Mar 1935 - Sep 2020	Cfb
Eu-272	4096	Flensburg (Schäferhaus)	Europe	41	54.777	9.377	Jan 1946 - Sep 2020	Cfb
Eu-273	4107	Frankfurt/Main (Feldbergstr.)	Europe	109	50.123	8.661	Jul 1935 - Sep 2020	Cfb
Eu-274	4114	Freiburg	Europe	236	48.024	7.835	May 1949 - Sep 2020	Cfb
Eu-275	4129	Gardelegen	Europe	47	52.514	11.398	Mar 1952 - Sep 2020	Cfb
Eu-276	4131	Garmisch-Partenkirchen	Europe	719	47.484	11.063	Jan 1936 - Sep 2020	Dfb
Eu-277	4134	Geisenheim	Europe	110	49.985	7.954	Jan 1927 - Sep 2020	Cfb
Eu-278	4141	Genthin	Europe	35	52.389	12.163	Feb 1957 - Sep 2020	Cfb
Eu-279	4147	Glucksburg-Meierwik	Europe	27	54.849	9.508	Jan 1946 - Sep 2020	Cfb
Eu-280	4151	Göttingen	Europe	167	51.502	9.953	Mar 1947 - Sep 2020	Cfb
Eu-281	4152	Goldberg	Europe	58	53.607	12.104	Jan 1951 - Sep 2020	Dfb
Eu-282	4171	Grunow	Europe	56	53.317	13.936	Jan 1973 - Sep 2020	Dfb
Eu-283	4184	Hamburg-Sankt Pauli	Europe	35	53.548	9.97	Sep 1938 - Sep 2020	Cfb
Eu-284	4185	Artern	Europe	164	51.376	11.293	Apr 1958 - Sep 2020	Dfb
Eu-285	4194	Harzgerode	Europe	404	51.653	11.138	Jan 1948 - Sep 2020	Dfb
Eu-286	4217	Bad Hersfeld	Europe	272	50.853	9.738	Aug 1953 - Sep 2020	Cfb
Eu-287	4236	Hohn	Europe	10	54.313	9.539	Oct 1981 - Jul 2009	Cfb
Eu-288	4265	Jever	Europe	7	53.532	7.881	Jan 1940 - Jul 2004	Cfb
Eu-289	4273	Kall-Sistig	Europe	505	50.503	6.527	Jan 1979 - Sep 2020	Cfb
Eu-290	4275	Kaltennordheim	Europe	487	50.628	10.147	Feb 1951 - Mar 2003	Dfb
Eu-291	4281	Kiel-Kronshagen	Europe	17	54.339	10.094	Jan 1940 - Jun 2019	Cfb
Eu-292	4285	Bad Kissingen	Europe	282	50.226	10.08	Jan 1947 - Sep 2020	Dfb
Eu-293	4288	Kleiner Feldberg/Taunus	Europe	826	50.223	8.448	Jan 1936 - Sep 2020	Dfb
Eu-294	4294	Klippeneck	Europe	973	48.106	8.756	Jan 1947 - Sep 2020	Dfb

Eu-295	4318	Kyritz	Europe	40	52.938	12.411	May 1992 - Sep 2020	Dfb
Eu-296	4338	Leck	Europe	7	54.793	8.949	Jan 1954 - Sep 2020	Cfb
Eu-297	4343	Leinefelde	Europe	356	51.385	10.302	Jan 1957 - Sep 2020	Dfb
Eu-298	4344	Leipzig-Holzhausen	Europe	138	51.316	12.448	Jan 1931 - Sep 2020	Dfb
Eu-299	4352	Lichtenhain-Mittelndorf	Europe	321	50.939	14.211	Jun 1994 - Sep 2020	Dfb
Eu-300	4353	Barth	Europe	3	54.341	12.711	Jan 1976 - Sep 2020	Cfb
Eu-301	4360	Lingen	Europe	22	52.519	7.308	Jan 1951 - Jun 2020	Cfb
Eu-302	4363	Baruth	Europe	55	52.062	13.503	Jan 1998 - Sep 2020	Cfb
Eu-303	4371	Lubeck	Europe	15	53.879	10.693	Mar 1950 - Sep 2020	Cfb
Eu-304	4372	Lubeck-Blankensee	Europe	5	53.811	10.707	Mar 1950 - Sep 2020	Cfb
Eu-305	4374	Luchow	Europe	17	52.974	11.139	Dec 1954 - Sep 2020	Cfb
Eu-306	4376	Ludenscheid	Europe	387	51.247	7.643	Jan 1994 - Sep 2020	Cfb
Eu-307	4386	Manschnow	Europe	12	52.548	14.548	Mar 1992 - Sep 2020	Cfb
Eu-308	4389	Marienberg	Europe	639	50.652	13.148	Jan 1975 - Sep 2020	Dfb
Eu-309	4390	Bad Marienberg	Europe	547	50.663	7.959	Dec 1962 - Sep 2020	Dfb
Eu-310	4414	Michelstadt-Vielbrunn	Europe	453	49.719	9.101	Oct 1987 - Sep 2020	Cfb
Eu-311	4419	Beerfelden	Europe	450	49.563	8.969	Dec 1950 - Jul 2004	Dfb
Eu-312	4428	Muhldorf	Europe	405	48.28	12.504	Jan 1953 - Sep 2020	Dfb
Eu-313	4430	Muncheberg	Europe	63	52.519	14.125	Jan 1951 - Sep 2020	Dfb
Eu-314	4440	Belm	Europe	103	52.318	8.171	Feb 1952 - Sep 2020	Cfb
Eu-315	4443	Neubrandenburg	Europe	81	53.548	13.193	Jul 1976 - Sep 2020	Dfb
Eu-316	4447	Bendorf	Europe	127	50.414	7.589	Jan 1990 - Sep 2011	Cfb
Eu-317	4450	Neuhaus Am Rennweg	Europe	845	50.501	11.136	Jan 1991 - Aug 2019	Dfb
Eu-318	4497	Oldenburg	Europe	11	53.178	8.182	Jan 1947 - Oct 2012	Cfb
Eu-319	4498	Oschatz	Europe	150	51.297	13.094	Jan 1983 - Sep 2020	Cfb
Eu-320	4499	Osnabruck	Europe	95	52.257	8.054	Feb 1952 - Sep 2020	Cfb
Eu-321	4500	Osterfeld	Europe	246	51.088	11.931	Feb 1992 - Sep 2020	Cfb
Eu-322	4522	Plauen	Europe	386	50.483	12.132	Jan 1935 - Sep 2020	Dfb
Eu-323	4531	Putbus	Europe	40	54.366	13.478	May 1958 - Sep 2020	Dfb
Eu-324	4537	Quickborn	Europe	13	53.734	9.878	Jan 1947 - Jun 2020	Cfb
Eu-325	4544	Kr. Ravensburg Weingarten	Europe	440	47.807	9.622	Feb 1946 - Sep 2020	Dfb
Eu-326	4570	Berlin-Schonefeld	Europe	46	52.382	13.533	Mar 1992 - Sep 2020	Dfb
Eu-327	4591	Bad Salzuflen	Europe	135	52.106	8.753	Feb 1936 - Sep 2019	Cfb
Eu-328	4605	Schierke	Europe	609	51.767	10.655	Mar 1935 - Apr 2020	Dfb
Eu-329	4607	Schleiz	Europe	501	50.571	11.806	Nov 1991 - Sep 2020	Dfb
Eu-330	4617	Schmucke	Europe	937	50.656	10.771	Jul 1978 - Sep 2020	Dfb
Eu-331	4634	Berus	Europe	363	49.265	6.688	Jan 1951 - Sep 2020	Cfb

Eu-332	4637	Seehausen	Europe	21	52.893	11.731	Oct 1976 - Sep 2020	Cfb
Eu-333	4652	Soltau	Europe	76	52.962	9.797	Jul 1947 - Sep 2020	Cfb
Eu-334	4655	Sonneberg-Neufang	Europe	626	50.376	11.184	Jan 1951 - Jun 2008	Dfb
Eu-335	4676	Teterow	Europe	38	53.763	12.558	Jul 1954 - Sep 2020	Dfb
Eu-336	4680	Tholey	Europe	386	49.474	7.039	Jun 1975 - Sep 2020	Cfb
Eu-337	4692	Travemunde	Europe	2	53.964	10.891	Oct 1946 - Sep 2001	Cfb
Eu-338	4698	Trollenhagen	Europe	69	53.602	13.306	Jul 1976 - Sep 2020	Dfb
Eu-339	4705	Ueckermunde	Europe	1	53.746	14.069	Aug 1992 - Sep 2020	Dfb
Eu-340	4708	Ulm	Europe	567	48.384	9.954	Aug 1950 - Sep 2014	Dfb
Eu-341	4709	Ummendorf	Europe	162	52.162	11.177	Mar 1947 - Sep 2020	Cfb
Eu-342	4726	Ahrensburg-Wulfsdorf	Europe	46	53.664	10.2	Jan 1961 - Dec 2001	Cfb
Eu-343	4734	Waren	Europe	70	53.521	12.669	May 1955 - Sep 2020	Dfb
Eu-344	4741	Weihenstephan-Durnast	Europe	477	48.403	11.696	Jul 1936 - Sep 2020	Dfb
Eu-345	4743	Weimar	Europe	264	50.976	11.309	Jun 1949 - Jun 2007	Dfb
Eu-346	4745	Weinbiet	Europe	553	49.377	8.123	Apr 1953 - Sep 2020	Dfb
Eu-347	4750	Weissenburg	Europe	422	49.02	10.962	Jul 1947 - Sep 2020	Dfb
Eu-348	4758	Wernigerode	Europe	234	51.848	10.769	Feb 1951 - Sep 2020	Cfb
Eu-349	4763	Bocholt (Marienschule)	Europe	25	51.839	6.611	Jan 1947 - Feb 2006	Cfb
Eu-350	4766	Wiesenburg	Europe	187	52.122	12.46	May 1992 - Sep 2020	Dfb
Eu-351	4767	Bocholt	Europe	21	51.831	6.536	Jan 1947 - Feb 2006	Cfb
Eu-352	4776	Wittenberg	Europe	105	51.89	12.646	Sep 1953 - Sep 2020	Dfb
Eu-353	4801	Zinnwald-Georgenfeld	Europe	877	50.733	13.753	Jan 1971 - Sep 2020	Dfb
Eu-354	4815	Boizenburg	Europe	45	53.393	10.689	Jan 1951 - Sep 2020	Cfb
Eu-355	4818	Schönhagen (Ostseebad)	Europe	2	54.641	10.024	Jan 1998 - Sep 2020	Cfb
Eu-356	4820	Boltenhagen	Europe	15	54.004	11.192	Jan 1947 - Sep 2020	Cfb
Eu-357	4839	Dornick	Europe	26	54.167	10.354	Jan 1950 - Sep 2020	Cfb
Eu-358	4879	Braunlage	Europe	607	51.725	10.604	Mar 1935 - Apr 2020	Dfb
Eu-359	4882	Braunschweig	Europe	81	52.29	10.448	Jan 1931 - Sep 2020	Cfb
Eu-360	4885	Bremerhaven	Europe	7	53.534	8.577	Jan 1949 - Sep 2020	Cfb
Eu-361	4888	Bremervorde	Europe	3	53.499	9.173	Jan 1947 - Sep 2020	Cfb
Eu-362	4941	Buckeburg	Europe	68	52.282	9.088	Jan 1979 - Aug 2020	Cfb
Eu-363	4950	Carlsfeld	Europe	897	50.432	12.613	Mar 1995 - Sep 2020	Dfb
Eu-364	4952	Celle	Europe	39	52.595	10.028	Jan 1940 - Feb 2007	Cfb
Eu-365	4954	Chemnitz	Europe	418	50.793	12.873	Apr 1938 - Sep 2020	Dfb
Eu-366	4958	Lautertal-Oberlauter	Europe	345	50.308	10.969	Jan 1955 - Sep 2020	Dfb
Eu-367	4970	Deuselbach	Europe	481	49.763	7.056	Jan 1951 - Sep 2020	Cfb
Eu-368	4971	Diepholz	Europe	39	52.59	8.346	Jan 1994 - Sep 2020	Cfb

Eu-369	4993	Landvik	Europe	6	58.34	8.523	Mar 1987 - Dec 2020	Dfb
Eu-370	5039	Fiskabygd	Europe	41	62.103	5.582	Jan 1969 - Sep 2020	Cfb
Eu-371	5093	Loken I Volbu	Europe	521	61.122	9.063	Jun 1987 - Dec 2020	Dfc
Eu-372	8555	Wageningen - Veenkampen	Europe	5	51.981	5.622	Mar 1928 - Aug 2020	Cfb
Eu-373	10961	Voorschoten	Europe	-1	52.139	4.436	Sep 1951 - Sep 2020	Cfb
Eu-374	11249	Orly	Europe	89	48.717	2.384	Jan 1978 - Jun 2020	Cfb
Eu-375	11367	Tartu-Toravere	Europe	70	58.264	26.461	Jan 1955 - Dec 2020	Dfb
Eu-376	11748	Greifswald-Wieck	Europe	0	54.1	13.45	Feb 1936 - Sep 2020	Dfb
Eu-377	11776	Neuglobsow (Hm)	Europe	6	53.142	13.032	Jan 1967 - Sep 2004	Dfb
Eu-378	17902	Maribor - Vrbanski Plato	Europe	279	46.568	15.626	Jun 1997 - Sep 2020	Dfb
Eu-379	18015	As	Europe	92	59.661	10.782	Jan 1959 - Sep 2020	Dfb
Eu-380	18017	Kvithamar	Europe	27	63.488	10.879	Jan 1982 - Sep 2020	Dfb
Eu-381	18018	Tjotta	Europe	21	65.829	12.426	Jul 1987 - Dec 2020	Dfb
Eu-382	18020	Tromso - Holt	Europe	20	69.654	18.909	Jun 1987 - Nov 2020	Dfc
Eu-383	18059	Frosta	Europe	32	63.565	10.693	Jan 1982 - Sep 2020	Dfb
Eu-384	18811	Trondheim - Tyholt	Europe	113	63.423	10.43	Jan 1952 - Sep 2020	Dfc
Eu-385	18817	Bjoerkehaug I Jostedal	Europe	305	61.659	7.276	Jan 1963 - Sep 2020	Dfc

*Köppen class was estimated using the raw data of stations based on the criteria of [Table 2.1](#).